NAVAL POSTGRADUATE SCHOOL
MONTEREY, CALIFORNIA

THESIS

EVALUATION OF EFFECTIVE MDTD/MRTD FOR FLIR FROM PREOS92 MEASUREMENT DATA

by

Fu-Chau Liu

June 1996

Thesis Advisor: Alfred W. Cooper

Approved for public release; distribution is unlimited.

19961024 024

1. AGENCY USE ONLY *(Leave blank)*	2. REPORT DATE June 1996	3. REPORT TYPE AND DATES COVERED Master's Thesis	
4. TITLE AND SUBTITLE EVALUATION OF EFFECTIVE MDTD/MRTD FOR FLIR FROM PREOS92 MEASUREMENT DATA		5. FUNDING NUMBERS	
6. AUTHOR(S) Fu-Chau Liu			
7. PERFORMING ORGANIZATION NAME(S) AND ADDRESS(ES) Naval Postgraduate School Monterey, CA 93943-5000		8. PERFORMING ORGANIZATION REPORT NUMBER	
9. SPONSORING/MONITORING AGENCY NAME(S) AND ADDRESS(ES)		10. SPONSORING/MONITORING AGENCY REPORT NUMBER	

11. SUPPLEMENTARY NOTES The views expressed in this thesis are those of the author and do not reflect the official policy or position of the Department of Defense or the U.S. Government.

12a. DISTRIBUTION/AVAILABILITY STATEMENT Approved for public release; distribution is unlimited.	12b. DISTRIBUTION CODE

13. ABSTRACT (maximum 200 words)

This thesis addresses the evaluation of the apparent target-background temperature difference (ΔT_{app}) at maximum range and compares ΔT_{app} with MDTD/MRTD of a typical FLIR system. The atmospheric propagation code (SEARAD) and Planck's radiation law were employed to obtain atmospheric transmittance and path radiance. The atmospheric parameters were selected as close to the aircraft overflights as possible using PREOS 92 data as inputs of the SEARAD code. Ship target (R/V POINT SUR) modeling was established for MDTD/MRTD evaluation using a rectangular parallelepiped model of the ship's physical length, width and height. The geometry data for MDTD/MRTD evaluations were also selected from the PREOS 92 experiment measurement set. The MDTD/MRTD functions for a generic FLIR in wide field of view (WFOV) application were deduced from Shumaker. Johnson criterion was employed as a detection criterion. Resolution line-pairs at detection range to resolve the target have also been evaluated and compared against Johnson Criterion.

The temperature differences between ΔT_{app} and MDTD at detection range show large scatter, ranging from 5% to 600 %. They also show agreement with the same sensor altitude and viewing angle. A comparison of ΔT_{app} with MRTD at classification range and identification range show that using NFOV would be more appropriate for target classification/recognition. Resolution line-pairs at detection range derived from a typical WFOV MRTD curve show 10%~50% error for the eight runs, which is acceptable as compared against Johnson Criterion quoted as 1 ± 0.25 mRad.

14. SUBJECT TERM : MDTD, MRTD, PREOS92	15. NUMBER OF PAGES **122**
	16. PRICE CODE

17. SECURITY CLASSIFICATION OF REPORT Unclassified	18. SECURITY CLASSIFICATION OF THIS PAGE Unclassified	19. SECURITY CLASSIFICATION OF ABSTRACT Unclassified	20. LIMITATION OF ABSTRACT UL

EVALUATION OF EFFECTIVE MDTD/MRTD FOR FLIR FROM PREOS92 MEASUREMENT DATA

Fu-Chau Liu
Captain, Republic of China Army
B.S., Chung-Cheng Institute of Technology-1988

Submitted in partial fulfillment
of the requirements for the degree of

**MASTER OF SCIENCE
IN
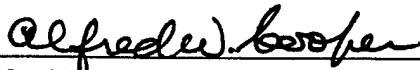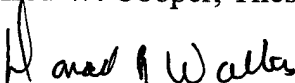Applied Physics (Electro-Optics)**

from the
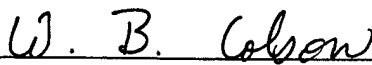
**NAVAL POSTGRADUATE SCHOOL
June 1996**

Author: _____
Fu-Chau , Liu

Approved by: _____
Alfred W. Cooper, Thesis Advisor

_____
Donald L. Walters, Co-Advisor

_____
William B. Colson , Chairman
Department of Physics

ABSTRACT

This thesis addresses the evaluation of the apparent target-background temperature difference (ΔT_{app}) at maximum range and compares ΔT_{app} with MDTD/MRTD of a typical FLIR system. The atmospheric propagation code (SEARAD) and Planck's radiation law were employed to obtain atmospheric transmittance and path radiance. The atmospheric parameters were selected as close to the aircraft overflights as possible using PREOS 92 data as inputs of the SEARAD code. Ship target (R/V POINT SUR) modeling was established for MDTD/MRTD evaluation using a rectangular parallelepiped model of the ship's physical length, width and height. The geometry data for MDTD/MRTD evaluations were also selected from the PREOS 92 experiment measurement set. The MDTD/MRTD functions for a generic FLIR in wide field of view (WFOV) application were deduced from Shumaker. Johnson criterion was employed as a detection criterion. Resolution line-pairs at detection range to resolve the target have also been evaluated and compared against Johnson Criterion.

The temperature differences between ΔT_{app} and MDTD at detection range show large scatter, ranging from 5% to 600 %. They also show agreement with the same sensor altitude and viewing angle. A comparison of ΔT_{app} with MRTD at classification range and identification range show that using NFOV would be more appropriate for target classification/recognition. Resolution line-pairs at detection range derived from a typical WFOV MRTD curve show 10%~50% error for the eight runs, which is acceptable as compared against Johnson Criterion quoted as 1 ± 0.25 mRad.

TABLE OF CONTENTS

x

LIST OF FIGURES

LIST OF TABLES

ACKNOWLEDGMENT

I. INTRODUCTION

Infrared (IR) systems have been under development continually over the past decade. IR systems are usually used for target search, detection, classification and identification. The performance of many military systems using FLIR technology is strongly dependent on environmental conditions in the tactical operation area. The crucial performance parameter of a FLIR system sensor is its maximum detection range (MDR) for a specific target. MDR is determined by application of a defined apparent temperature difference (ΔT) criterion for detection or recognition/classification at a selected probability. A generic tactical scenario situation is shown in Figure 1 when an airborne FLIR sensor detects a ship at a certain distance. In order to predict the MDR, it is necessary to determine the target minus the background temperature contrast (ΔT) as viewed by the sensor. To be detected the point target ΔT must equal the Minimum Detectable Temperature Difference (MDTD) or Minimum Resolvable Temperature Difference (MRTD) of the FLIR system. The temperature contrast calculation requires an accurate prediction of the spectral radiance of the target and the background, and the attenuation and radiance of the path between the sensor and the target. From experience we know that the meteorological conditions have a great influence on the performance of FLIR systems. Over the past several decades several atmospheric propagation codes (HITRAN, MODTRAN and LOWTRAN) were developed by the Phillips Laboratory for both high resolution and low resolution transmission. The HITRAN codes, for example, FASCODE, have very high resolution and resolve individual molecular rotation , vibration lines. But they are slow and expensive. LOWTRAN (the latest version is LOWTRAN 7) is essentially a curve fitting match to empirical data. It was designed to calculate atmospheric transmittance and radiance averaged over a 20 inverse centimeter frequency interval with steps at multiples of 5 inverse centimeters, and accuracy about 10 %. This is a faster code and has received wide acceptance. MODTRAN is an atmospheric propagation code that can be used at moderate resolution, to 2 cm^{-1}, using data stored at 1

1

cm intervals. MODTRAN2 also extends the spectral range to include the near ultraviolet through the microwave. Recently, a new research atmospheric propagation code called "SEARAD" (modified MODTRAN2) has also been developed to predict the transmittance, path radiance, and sea and reflected sky radiances [Ref. 1]. SEARAD code adds sea surface radiance based on Cox-Munk (Cox and Munk, 1954, 1956) statistical model [Ref. 1] which also includes sun glint effects. It is a DOS-compatible program which can run on a personal computer and calculates sea radiance.

This thesis will address the calculation of the apparent ΔT at maximum range and compare ΔT with MDTD/MRTD to examine the influence of the meteorological parameters that cause a variance in FLIR performance. The source of meteorological parameters was based on the PREOS92 experiment that was conducted on August 04, 1992. The PREOS computer program [Ref. 2] is a NRaD developmental Tactical Decision Aid (TDA) model that was intended as a range prediction technique for airborne FLIR systems. PREOS92 represents an experiment for validation of the PREOS program conducted off the California coast from Monterey in 1992. Details of this experiment will be described in Chapter III. In this experiment, The research vessel POINT SUR (R/V POINT SUR) was used as a target and as a measurement platform. The skin temperature distribution was recorded throughout the experiment using a set of 15 thermistors on the ship skin. Thermal image data obtained from the R/V POINT SUR measured from navy aircraft were used with the ship temperature data to determine the average ship temperature. Detection range, classification range and identification range were determined by military aircraft overflights. Meteorological and sea surface data measured on board the POINT SUR were used as inputs to the atmospheric propagation computations. A Radon counting instrument on the R/V POINT SUR was used to determine the air mass parameter (ICSTL) representing the degree of coastal aerosol influence for inclusion in the SEARAD propagation code. In this experiment, the NRaD aircraft, the military aircraft and the radiosonde balloons could not occupy the air space around the R/V POINT SUR at the same time. The experiment was planned to have data

2

from those sources as closely spaced in time as possible. The meteorological parameters, observed detection ranges and aircraft altitudes selected in this experiment were used as inputs to the "SEARAD" code to calculate the atmospheric infrared (8 to 12 μm) transmittance and path radiance.

The objective of the calculation of apparent temperature difference (ΔT) was to evaluate the effective Minimum Detectable Temperature Difference (MDTD) and Minimum Resolvable Temperature Difference (MRTD) for the FLIR system from the PREOS 92 measurement set. The Johnson criterion, the number of line pairs need across a target, was used for evaluating the MDTD/MRTD of the FLIR system. The ΔT calculation was based on the meteorological data collected that was closest in time to the aircraft overflights on the test. After accessing the transmittance and path radiance calculated from SEARAD, Planck's radiation law was applied to find the apparent radiance difference and corresponding temperature difference (ΔT) at the detection range. Generic FLIR parameters were used to estimate MDTD/MRTD of the FLIR sensor. Furthermore, the number of line pairs required to satisfy the MRTD criterion at the detection range were investigated to improve the performance of prediction.

II. THEORY AND BACKGROUND

A. DETECTION SCENARIO

Figure 1 shows a typical scenario to detect a ship with an airborne FLIR. [Ref. 2] In order to model the detection of the ship, we have to know or calculate the detected radiance seen by the sensor, after propagation through the atmosphere. From this we can compute an apparent temperature difference ΔT from the ship and background and compare this to the Minimum Detectable Temperature Difference (MDTD) or Minimum Resolvable Temperature Difference (MRTD). If the apparent temperature difference is equal to the MDTD or MRTD, the target should be detected or resolved.

In order to find the apparent temperature differences between ship and background, the ship and the background radiance must be adjusted for the atmospheric effects over the spectrum of the sensor, and then the effective temperature difference calculated. The ship radiance must be adjusted by the transmittance and path radiance effects. Also, the background flux has to be adjusted for path radiance, sea surface radiance and reflected sky radiance. [Ref. 2, p. 3]

B. RADIATION LAW

The following thermal radiation laws were used for the IR radiation and apparent temperature difference calculations. These equations are in general use and are summarized in Ref. 3 and Ref. 4. They are reproduced here for convenience.

1. Planck's Blackbody Radiation Law

A blackbody is an idealized source of radiant energy. The emitted energy depends on the temperature of the object and the wavelength. The spectral radiant emittance from a blackbody is given by Planck's blackbody law and is shown in Equation (1),

$$M(\lambda,T) = \left(\frac{2\pi hc^2}{\lambda^5}\right)\left(\frac{1}{e^{\frac{hc}{\lambda kT}} - 1}\right) \tag{1}$$

5

where

λ = wavelength (m),

k = Boltzmann's constant = 1.38×10^{-23} (W - sec / K),

h = Planck's constant = 6.626×10^{-34} (W - sec^2),

T = temperature (K).

Planck's law can be applied to all FLIR systems and is valid for the entire electromagnetic spectrum. The spectral radiant emittance of a blackbody ranging from 500 to 900 K is shown in Figure 2. [Ref. 3, p. 55] From this figure it shows that the spectral radiant emittance dependents on the temperature of the object and the wavelength.

2.   Stefan-Boltzmann Law

Integrating $M(\lambda,T)$ over all wavelengths gives the total radiant exitance M_λ, Equation (2), from a blackbody surface in terms of temperature T.

$$M_\lambda = \sigma T^4, \tag{2}$$

where

σ = Stefan-Boltzmann constant = 5.6697×10^{-8} (W/m^2/K^4)

For a non-blackbody source, this law is modified by the effective source emissivity ε, giving the form in Equation (3)

$$M = \varepsilon \sigma T^4. \tag{3}$$

For in-band radiance, the radiance N can be calculated using the universal blackbody curve as shown in Figure 3 or the proportional radiation table (Appendix A) with Equation (4) [Ref. 5].

$$N = \frac{\varepsilon \sigma T^4}{\pi} \Delta q, \tag{4}$$

where

ε = emissivity of the source.

Δq = difference of two q values from the proportional radiation table (Appendix A)

6

The proportional radiation $q = f(\lambda, T)$ represents the fraction of the radiant exitance emitted by a blackbody at temperature T at all wavelengths up to the selected value of λ. It can be described in Equation (5):

$$q = \frac{\int_0^\lambda M(\lambda, T)d\lambda}{\int_0^\infty M(\lambda, T)d\lambda} \quad .$$

(5)

If q values are not shown on the table, they can be calculated by interpolation between two q value entries.

3.   Lambert-Beer Law

The atmospheric transmittance is a strong function of wavelength, which can be described by the Lambert-Beer law.

$$\tau(\lambda) = e^{-\mu R} \quad ,$$

(6)

where

$\tau(\lambda)$ = spectral atmospheric transmittance,
λ = wavelength,
$\mu(\tau)$ = extinction coefficient,
R = path length.

The extinction coefficient depends on the atmospheric molecular composition and aerosol concentration. It is very sensitive to the specific frequencies of the molecular vibration and rotation transitions.

4.   Absorption and Scattering

The infrared radiation will attenuate as it propagates through the atmosphere by the processes of absorption and scattering. The attenuation is characterized by the total extinction coefficient.

$$\mu = \mu_a + \mu_s \quad ,$$

(7)

where

7

μ = total extinction coefficient,

μ_a = extinction coefficient for total absorption,

μ_S = extinction coefficient for total scattering.

Both the scattering and absorption coefficients have two components; one from the molecules of the air and the other from aerosol particles suspended in it. Scattering by aerosols and molecules has a large effect in the visible region, while absorption dominates in the infrared region of the electromagnetic spectrum. Since FLIR systems are designed to operate between 8 to 12 μm, it is important to predict the transmittance of the atmosphere as a function of wavelength and weather conditions. These two coefficients are shown in Equation (8) and (9).

$$\mu_a = k_m + k_a \ , \qquad\qquad\qquad (8)$$

$$\mu_S = \sigma_m + \sigma_\alpha \qquad\qquad\qquad (9)$$

where

k_m = molecular absorption coefficient,

k_a = aerosol absorption coefficient,

σ_m = molecular scattering coefficient,

σ_α = aerosol scattering coefficient.

The relative values of the four coefficients depend strongly on the density and molecular composition of the atmosphere and the composition and size distribution of the aerosols. [Ref. 6, p.12-7]

A range of computer models have been developed for computation of atmospheric transmittance for various defined meteorological scenarios. These models include LOWTRAN, MODTRAN and FASCODE. Recent variations of these codes, for example SEARAD, also compute path radiance, and the background radiance can be converted into background temperature directly. [Ref. 1]

C.   RADIATION IN TDA MODELING

A Tactical Decision Aid (TDA) code such as a FLIR range prediction generally consists of three models:

- A target model which describes a target as an average temperature difference ΔT against a background.

- An atmosphere model which describes the radiation in apparent temperature difference from the target to the sensor.

- A detection model describes the sensor performance for specifying MDTD for detection or MRTD for classification or recognition. [Ref. 7]

The PREOS model predicts the maximum detection range of an airborne FLIR system over the 8 to 12 micron band. [Ref. 2] In this model, the SHIPSIG model provides the ship target signature based on ship skin temperatures and meteorological data. The target signature appears as an average temperature between the ship and the background. A modified form of the LOWTRAN6 model computes the propagation of the radiation difference to the detection range. A parameterized MDTD equation based on a known system performance represents the FLIR characteristics.

The following equations and definitions to describe TDA modeling are taken from C.P. McGrath [Ref. 2, pp. 3-6], Jon C. Kreitz [Ref. 3, p. 12-15] and C.R.Zeisse [Ref. 1, p. 7]

1. Target Model

Typically a target model consists of an average ship temperature and the difference from the adjacent background temperature ΔT_o. To incorporate atmospheric changes in this quantity it must be converted into an equivalent radiance difference. This is done through an integration over Planck's blackbody distribution over the system bandwidth and gives a zero range equivalent in-band blackbody radiance $N(H,\theta)_s$ for the target, where H represents the altitude of a FLIR sensor and θ represents the elevation angle from the target to the sensor. An equivalent radiance for the background must be included.

2. Atmosphere Model

The atmosphere model computes the path transmittance, the path radiance (e.g from SEARAD) and the background radiance $N(H, \theta)_b$. $N(H, \theta)_b$ is the sum of the three radiance terms:

- Sea Surface Radiance $N(H, \theta)_{ss}$;

- Reflected Sky Radiance $N(H, \theta)_{rsk}$;

- Path Radiance $N(H, \theta)_p$.

These three terms may be calculated from the modified MODTRAN2 (SEARAD) code, and can be described by Equation (10).

$$N\left(H, \theta\right)_b = N\left(H, \theta\right)_{SS} + N\left(H, \theta\right)_{rsk} + N\left(H, \theta\right)_P \tag{10}$$

Also the radiance of the background has been converted directly to an equivalent background temperature by the SEARAD code. [Ref. 1]

3. Detection Model

The detection model compares the apparent temperature difference ΔT_{app} (H, θ), which varies with the range and viewing angle, to the threshold parameter of the sensor. $\Delta T_{app}(H, \theta)$ is the apparent target minus background temperature difference seen by an infrared sensor, and is a function of the sensor's altitude H and viewing angle θ relative to the zenith. It can be described by Equation (11)

$$\Delta T\left(H, \theta\right)_{app} = T\left(H, \theta\right)_{S+P} - T\left(H, \theta\right)_b \tag{11}$$

where

$T\left(H, \theta\right)_{S+P}$ = average apparent target temperature,

$T\left(H, \theta\right)_b$ = average background temperature.

The major purpose of this calculation is to deduce the apparent temperature difference ΔT_{app} at the observed detection range, and compare this with the MDTD/MRTD of the

aircraft FLIR sensor, to evaluate the effectiveness of the MDTD/MRTD criteria for the FLIR system.

D. DETECTION CRITERION

1. Introduction

The target characteristics play an important role in a FLIR system analysis. The primary reason for describing the properties of targets is to provide a basic detection criterion for analyzing the interaction of the target and the FLIR system. Two parameters frequently used to characterize targets for purposes of calculating their interaction with FLIR systems are the "critical dimension" and "average effective temperature difference." An "aperiodic" detection criterion is sometimes used, meaning that the irradiance at one pixel in the scene exceeds a defined threshold to be identified as a target, with no minimum number of resolvable line pairs on the image. These target features provides a way to deduce the ability of an observer using a FLIR to obtain information regarding scenes, objects and targets from their displayed images. However, other analyses believe that some level of resolution above one scan line of the target compared with the background is necessary for detection.

2. Target Transform Function

Laboratory measurements will describe the performance of the FLIR-aided eye in the detection of an isolated rectangular temperature target or resolution of the bars in a standard "bar pattern". Rectangular target detection is a form of "aperiodic detection", characterized by a FLIR parameter called the Minimum Detectable Temperature Difference (MDTD). Resolving a bar chart represents "periodic detection" and is characterized by a FLIR parameter called the Minimum Resolvable Temperature Difference (MRTD). [Ref. 8, pp. 2.1-2.4] These two parameters will be described in detail in the next section.

Evaluating the field performance of a FLIR requires the selection of an idealized target to characterize a particular visual task. This is a judgmental problem for which no firm rules are established. In general, detection of a real target is equivalent to detection

11

of an isolated rectangle whose area is equal to the target area and whose contrast temperature difference ΔT to the background is equal to the average ΔT between the actual target and background. Another visual discrimination capability involves resolving bars of a bar pattern whose ΔT between hot bars and cold bars is set equal to the average ΔT between the target and background, and whose spatial frequency is determined by the target's critical dimension and the task selected. It is helpful to represent real targets as idealized MDTD and MRTD test targets whose detectability/resolvability can be predicted and measured in the laboratory. [Ref. 8, p. 2-5]

3.   Equivalent Bar Chart Selection

Several criteria exist to relate the resolution of bar charts to levels of visual discrimination. The first one is the "Johnson Criterion," which has been widely used for land vehicle targets. [Ref. 8] In 1970, Johnson first put a set of tribar patterns next to a military target under different conditions. He used the minimum dimension of the target as a reference. [Ref. 8, p. 2-6] But Moser found that the Johnson Criterion was not suitable to ship targets. The Moser study involved many observations of cathode ray screen images of ship silhouettes formed of black squares of varied scale (representing "pixels"). These studies produced the following standard numbers of pixels needed for : detection (1 pixel), classification (66 pixels) and recognition (400 pixels). Shumaker relates the pixel criteria advanced by Moser to the equivalent bar chart spatial frequency. Moser found that the minimum ship dimension had little significance, but classification and identification of ships was related to the number of pixels falling within the area of a ship image. Table 1 shows the data relating the Moser and O'Neill conclusions to the Johnson criteria for detection, classification and recognition. Moser also found that the square root of projected area was "critical dimension" that gave consistent predictions for very elongated targets, while the "minimum dimension" led to incorrect conclusions. In lieu of prior target information, Moser recommended that this "average dimension" be used. [Ref. 8, pp. 2.6-2.10]

4.   Determination of Target Spatial Frequency

In FLIR performance analysis, the effective target area is the projected area normal to the line of sight from the sensor to the target. The area dependents on the target dimensions, the observing aspect and the obscuration of the target. The physical dimensions of a target must be known prior to performing radiometric calculations. Representing the target as a rectangular parallelepiped of dimension of a target's length, width and height simplifies subsequent calculations.

Another important consideration for FLIR analysis is the target aspect, the elevation angle θ and azimuth angle ϕ seen from the front view. The area of a target image as a function of its dimension and the azimuth and elevation angle is

$$A_T = lw \sin\theta + hw \cos\theta \sin\phi + hl \cos\theta \cos\phi \,, \tag{12}$$

where

h = the unobscured target height,

w = the target width,

ϕ = the target length,

l = the azimuth angle,

θ = the elevation angle.

Figure 4 shows the orientation of a ship target model for calculating the projected area.

Using Moser's suggestions the critical dimension D_c is then $D_C = \sqrt{A_T}$. Dividing the critical dimension D_c by the number of bars N in the bar chart gives the physical dimension χ to be resolved to accomplish the task, i.e. $\chi = D_c / N$.

Finally, the spatial frequency characterizing the target can be written as lines per milliradian

$$f_c = \frac{R}{2000\chi} \quad \text{(cyc/mRad)} \tag{13}$$

where R is the range in meters from sensor to target.[Ref. 8, pp. 10-16] The relation of the spatial frequency to range R and physical dimension χ are shown in Figure 5.

13

E. THE FLIR SYSTEM PERFORMANCE

The purpose of a FLIR system is to detect the arrival of IR energy, electronically process the detected energy, and display the results to the FLIR operator. The ability of the FLIR system to perform its function depends on how well it will provide a scene that the operator can view directly.

Two standard descriptions of FLIR performance are :

- Minimum Detectable Temperature Difference (MDTD)

- Minimum Resolvable Temperature Difference (MRTD)

Each of these provides a sensitivity measurement of the FLIR system. Both of them employ the concept of the Equivalent Blackbody Temperature of a non-blackbody object. The equivalent blackbody temperature is that temperature a blackbody must have to emit the same radiance as the target. This allows the use of a single value to represent the target's temperature and emissivity.

1. MRTD Description

MRTD is a function rather than a simple number. It gives the ΔT between the hot and ambient temperature bars of a standard 4 bar (7:1 aspect ratio) chart required to make the bars just resolvable as a function of the spatial frequency of the bars. MRTD is a measure of the performance of the entire FLIR system. Since the MRTD includes the observer, the measurement is subjective. [Ref. 8, p. 8-52] The MRTD can be written in terms of the Noise Equivalent Temperature Difference (NETD) and Modulation Transfer Function (MTF) of the FLIR system, the detector dwell time on a target point, and the required signal to noise ratio, but must also include a representation of the human operator perception factors which may be modeled as an eye filter function and integration time. [Ref. 8, pp. 8.37-8.38] It typically shows a rapid increase to an asymptotic value at a spatial frequency beyond which the pattern can not be resolved at any temperature difference. For a typical FLIR (Common Module), the instantaneous field of view (IFOV) is approximately 0.25 mRad so that the in-scan detector subtense Δx is approximately 0.25

mRad and the cut off spatial frequency (asymptote) is approximately $\dfrac{1}{\Delta x} = \dfrac{1}{0.25} = 4$ cyc/mRad. If we use the "rule of thumb" asymptote between $0.7/\Delta x$ and $0.9/\Delta x$, we would find that the asymptote is approximately 3 cyc/mRad. The effective IFOV depends on the magnification of the optics which may be variable in some FLIRs.

Shumaker gives a typical form for the MRTD. [Ref. 8, p. 8-52]

$$MRT(v) = \frac{2\ \text{SNRT}\ \text{NET}\ \rho_x^{\frac{1}{2}}}{\text{MTF}_S(v)}\left[\frac{v^2 \Delta x \Delta y}{L}\right]^{\frac{1}{2}}\left[t_e F_r N_{os} N_{ss}\right]^{-\frac{1}{2}}\ , \qquad (14)$$

where SNRT = signal to noise ratio threshold,

NET = noise equivalent temperature ,

ρ_x = noise filter factor,

Δx = in-scan detector subtense (mRad),

Δy = cross-scan detector subtense (mRad),

MTF = modulation transfer function,

v = spatial frequency for which MRT is desired in cyc/mRad,

L = length-to- width ratio of the bar (7),

t_e = eye integration time in second,

Fr = frame rate s^{-1},

N_{os} = overscan ratio,

N_{ss} = serial scan ratio.

Shumaker also provides an expression for the Noise Equivalent Temperature Difference (NET$_D$), [Ref. 8, pp. 8-7]

$$\text{NET}_D = \frac{10\left(\text{FOV}_x\ \text{FOV}_y\ F_r\ N_{os}\ N_{ss}\right)}{\left(\pi\ N_D \eta_{sc}\right)^{\frac{1}{2}} D \Delta x \Delta y D^{**} \eta_{cs}\ \frac{\partial N}{\partial T^{\tau_0}}}\ , \qquad (15)$$

where FOV$_x$ = in-scan FOV in mRad,

FOV$_y$ = cross-scan FOV in mRad,

N_D = number of detectors,

15

η_{sc} = scan efficiency,

$\partial N/\partial T$ = derivative of Planck's equation in W/cm^2 /K/Sr,

D^{**} = the band average detectivity in cm Hz$^{1/2}$ /W,

D = aperture diameter in meters,

τ_o = transmission of the optics.

For calculation purposes it is convenient to write MRTD as function of spatial frequency f in a parametric form.

$$MRTD = SL + \left(SC\left(\frac{2f}{\xi^{\frac{1}{2}}} \right) \exp\left(\frac{1}{2} \pi ER^2 f^2 \right) \right) \tag{16}$$

where SL (sensitivity limit), SC (sensitivity constant) and ER (Equivalent resolution) are FLIR constants derived for any given FLIR by fitting the equation above to the measured or calculated MRTD of the system for a 4 bar target pattern with ratio $\xi=7$ of bar length to width. [Ref. 9] FLIR constants are not generally available for specific FLIR instruments but can be deduced from suitable generic models. For example, Shumaker example 8-13 shows the typical FLIR parameters to model a generic FLIR system. [Ref. 8, p. 8-59] Figure 10 shows the relation between the MRTD and spatial frequency for a typical FLIR system. Since MRTD is a function of spatial frequency, the maximum range for classification or recognition is the range when the ship/background ΔT matches MRTD at the spatial frequency given by the appropriate criterion. (e.g., the Johnson criterion)

2. MDTD Description

The MDTD definition of a FLIR system is similar to the MRTD , but the target is represented as a large square and MDTD is not as dependent on the eye parameters. The definition of MDTD is the minimum detectable temperature difference between a large square target and its adjacent background that just makes the square target detectable. [Ref. 8, pp. 8.66-8.67] The square target represents a target of known angular subtense and temperature difference to the FLIR system. Also, the MDTD of a FLIR system can be

16

tabulated as a function of target angular subtense (TAS) for table look-up purposes. [Ref. 10, p.13-15]

Shumaker provides a typical form for MDTD

$$MDT(v) = \frac{(\text{SNRT})\,(\text{NET})\left(\Omega_T + r_s^2\right)(\Delta x \Delta y)^{\frac{1}{2}}}{\Omega_T\left[\frac{\pi}{4}\left(r_s^2 + r_B^2 + \Omega_T\right)t_e F_r N_{os} N_{ss}\right]^{\frac{1}{2}}} \quad , \tag{17}$$

where Ω_T = target angular subtense (mRad^2),

r_s = system resolution (mRad),

r_B = back-end resolution (mRad).

The other definitions of the parameters in Equation (17) such as SNRT, NET, Δx, Δy, t_e, F_r, N_{os}, N_{ss}, are the same as those in Equation (14).

The calculation of MDTD for a generic FLIR system can be described by a curve fit equation as shown in Equation (18). [Ref. 9]

$$MDTD = SL + \left(SC * \left(TAS^2 + ER^2\right)^{\frac{1}{2}} / TAS^2\right) \tag{18}$$

where SL , SC and ER are empirical FLIR constants as before. TAS represents the target angular subtense in mRad which equals 10^6 A_T/R^2. Figure 12 shows the relation between MDTD and target angular subtense (TAS) for a typical airborne FLIR system derived from equation (17) and equation (18) for WFOV application. This can be converted into a function of range for a specific target.

17

III. OVERVIEW OF PREOS 92 EXPERIMENT

A.   INTRODUCTION

The data for this thesis were obtained from an open ocean field experiment conducted from 27 July to 4 August 1992 off the coast of Monterey, California by Naval Command, Control and Ocean Surveillance Center (NCCOSC), Research, Development, Test and Evaluation Division (NRaD) in cooperation with the Naval Postgraduate School (NPS). The purpose of the experiment was to collect a comprehensive set of meteorological and ship temperature data, infrared images, and airborne FLIR detection range data to evaluate the Performance and Range of Electroptical System (PREOS) detection range algorithm developed at NCCOSC. Data and preliminary results of the PREOS comparison were documented by Kreitz [Ref. 3] and more completely by Hughes and McGrath. [Ref. 11]

The Research Vessel POINT SUR (R/V POINT SUR) was the primary target platform. R/V POINT SUR is a 135 foot ship (dimension : 41.5Lx9.75Wx8.8H (m)) owned by the National Science Foundation and operated by Moss Landing Marine Laboratory. It served as a platform for meteorological and surface measurements and as an infrared target for the airborne FLIR and imaging systems. Scientists from NPS, NRaD, and Naval Surface Warfare Center (NSWC) were aboard the POINT SUR to conduct the onboard measurements. Air temperatures ranged from 11.5 to 17.8° C during the measurement. Sea temperatures were from 11.0 to 18.1 °C. Wind speeds ranged from 3 to 26 knots. Stratus clouds dominated until the last day of the test when clear skies prevailed. The stratus base ranged from 140 m to 300 m according to the aircrew reports. Vertical profiles of atmospheric pressures, relative humidities, temperatures, and dew point were collected from radiosonde launches from the R/V POINT SUR. Due to the prevailing weather conditions the analysis of this thesis is applied only to the data of 4 August.

19

B. DATA MEASUREMENTS

1. Shipboard Measurements

Skin temperatures of the ship were collected from 15 thermistors attached to the ship, and a hand-held radiometer. The thermistors were mounted on the large area surfaces of the ship and were continuously recorded. Spot measurements of infrared skin temperature were made several times daily with a hand-held radiometer that operated in the 8 to 12 micron band. Meteorological data were collected by the NPS from a variety of ship board sensors. The parameters measured included wind speed, wind direction, relative humidity and pressure. Atmospheric radon concentrations were also recorded to determine the influence of continental versus marine air masses. The ship navigation data include latitude, longitude, gyro heading, and ship speed.

2. Airborne Measurements

The NRaD airborne platform was a Piper Navajo aircraft equipped with a thermal imaging recording system. The aircraft flew 11 missions. A total of 2603 image frames of POINT SUR were collected with the AGA 780 Radiometric Thermal Imaging System, which was operated in the 8 to 12 micron band.

3. FLIR Measurements

The R/V POINT SUR not only served as the primary meteorological measurement platform, but also was used as the target for the FLIR and AGA infrared imaging systems. Seven naval aircraft each employing an 8 to 12 μm FLIR system flew range detection missions during the experiment. Eight missions were flown, four at night, and four during the mid-morning, making a total of 57 passes at the target. The measured detection ranges, classification ranges and identification ranges during the overflights provide the primary foundation for evaluating the temperature difference transmitted to the FLIR sensor. During the detection runs, all detection ranges were determined using the wide field of view lens for common module FLIR systems with dual FOV. A target detection occurs when the aircraft operator first detected a dot on the display. This is a subjective

value. Display images were preserved on video tape which is now archived at NPS. [Ref. 3, 12]

IV. DATA SELECTION

The data utilized for the calculation of apparent temperature difference ΔT in this thesis were selected from the data gathered in the FLIR92 experiments. The data of the last day, 4 August 1992, were selected for use for the reasons outlined by Kreitz [Ref. 3], namely that the overcast conditions obtaining during the other overflights seriously impacted the application of the atmospheric propagation codes. Table 3 shows eight aircraft overflights conducted on 4 August, during the time period from 0411 to 0522 (GMT). Data from a radiosonde launch at 0401 (GMT) provides input information to the SEARAD code and are listed in Table 4. Table 5 shows the meteorological data needed for atmospheric propagation code (SEARAD). Atmospheric transmission and path radiance values obtained from the SEARAD code for calculating the apparent temperature difference at detection range, classification range and identification range are listed in Table 6, Table 7 and Table 8 separately. Table 3 shows the observed detection, classification and recognition ranges for eight flights that were used to evaluate the FLIR MDTD and MRTD. The average radiometric ship target temperatures corrected to zero range have been analyzed by Hughes and McGrath [Ref. 11] and are listed in Table 9. The meteorological data were selected to be as close as possible to the aircraft overflight time and provide a basis for apparent ΔT, MRTD and MDTD calculations. These data in Table 3, Table 4 and Table 5 served as inputs to the SEARAD code to obtain the transmittance and path radiance between the detection range, classification range and identification range from the aircraft to R/V POINT SUR.

V. ESTIMATION OF SYSTEM MDTD AND MRTD

To complete the comparison of apparent ΔT with the system requires numerical values of these quantities as functions of spatial frequency for the specific sensors used. Since this detailed information could not be obtained for the purposes of this thesis, suitable model functions were constructed using the available information. This section describes the generation of the comparison performance parameters.

From the widely distributed manuals on the Marine Patrol Aircraft sensor suites the FLIR was expected to be a Common Module type with 180 Mercury Cadmium Teluride detectors in parallel scan, with wide field of view (WFOV) 15^0 elevation and 20^0 azimuth, and 5^0 elevation and 6 ^{040}' azimuth in Narrow Field of View (NFOV). Moser [Ref. 13] has used detector angular subtense Δx of 0.25 mrad and Noise Equivalent Temperature 0.3 ^{0}C for such a system.

FLIRs of the Common Module generation have been discussed extensively by Shumaker [Ref. 8], Lloyd [Ref. 14] and Howe. [Ref. 15]

A.   GENERIC FLIR PARAMETERS FOR NFOV

The theoretical MRTD and MDTD can be expressed in Equation (14) and (17) discussed in Chapter II, Section E . [Ref. 8, p. 8-55]

$$MRT(v) = \frac{2\,\text{SNRT}\,\text{NET}\,\rho_x^{1/2}}{\text{MTF}_\text{S}(v)}\left[\frac{v^2\Delta x\Delta y}{L}\right]^{1/2}\left[t_e F_r N_{os} N_{ss}\right]^{-1/2} \tag{14}$$

$$MDT(v) = \frac{(\text{SNRT})\,(\text{NET})\left(\Omega_T + r_s^2\right)\left(\Delta x\Delta y\right)^{1/2}}{\Omega_T\left[\frac{\pi}{4}\left(r_s^2 + r_B^2 + \Omega_T\right)t_e F_r N_{os} N_{ss}\right]^{1/2}} \tag{17}$$

Shumaker provides the following set of parameters that are postulated to be appropriate to the Common Module FLIR in NFOV mode. [Ref. 9, p. 8-59]

FOV$_x$	6.86^0	FOV$_y$	5.16^0		L	7
F$_r$	30 sec^{-1}	N$_{os}$	1		r$_E$	0.3 mRad
N$_{ss}$	1	N$_D$	180		r$_d$	0.08
η_{sc}	0.75	τ_0	0.70		N$_s$	2
D	0.10 m	Δx	0.25 mRad		NET	0.1°K
Δy	0.25 mRad	D*	4×10^{10} cm Hz$^{1/2}$ /Watt			
f	0.20 m	MTF(v)	Tabulated below			
t$_e$	0.1 sec	SNRT	2.5			

MTF(v) calculation for NFOV

Spatial Frequency (v) (cyc/mRad)	Δx= 0.25 mRad MTF	1 mRad MTF
0.00	1.00	1.00
0.25	0.89	0.72
0.50	0.79	0.40
0.75	0.64	0.14
1.00	0.53	0.00
1.25	0.43	0.00
1.50	0.35	0.00
1.75	0.27	0.00
2.00	0.20	0.00
2.50	0.10	0.00
3.00	0.04	0.00

$\rho_x = (1 + (2v \bullet r_B)^2)^{-1/2}$ is computed from the equivalent back-end resolution r_B which is given for this example as 0.335 mRad. The NET calculated for this example system is 0.10 K. Following the reference in Moser this value would be replaced with NET =0.25 K. If a FLIR system has been used for a few years, the efficiency of the system will be degraded , and the NET will increase slightly. The choice of NET from 0.1 K to 0.25 K is reasonable. The resulting computation from the tabulated data for narrow field of view is shown in Figure 10.

B.   SELECTED COMPARISON FLIR PARAMETERS FOR WFOV

Since the range measurements were reported as being made in WFOV, Figure 11 shows an estimated MRTD for WFOV. In changing the optical field of view, changes will

occur in Δx and Δy, the detector angular subtenses, in ρ_x through the detector resolution, and in the system MTF. To obtain the required WFOV of 15^0 by 20^0 a linear magnification factor of 3 is required, giving detector angular subtense of Δx and Δy equal to 0.75 mRad. Shumaker also provides MDTD in Example 8-16, p. 8-59, with the set of parameters which are the same as for MRTD and considered to be appropriate to the Common Module FLIR in NFOV mode. The back-end resolution $r_B = (r_m^2 + r_d^2 + r_E^2)^{1/2}$ in this example is also given as 0.335 mRad. NET calculated in this example is also 0.1 °C. Since the range measurements were reported in WFOV, an equivalent MDTD as a function of Target Angular Subtense (TAS) for WFOV was also deduced and shown in Figure 12. As discussed before, a change of the optical field of view will change Δx and Δy, the detector angular subtense, as well as r_D, the detector resolution. To obtain the required WFOV, a linear magnification factor of 3 is also required, giving detector angular subtense of Δx and Δy equal to 0.75 mRad. The detector resolution r_D, which equals Δx, is also 0.75 mRad. The back-end resolution in WFOV with $\Delta x=0.75$ mRad will be 0.487 mRad. The following parameters which are postulated have been discussed above and selected to be appropriate to the Common Module FLIR in WFOV.

MTF(ν) calculation for WFOV

NET	0.125 °C	Spatial Frequency (ν) (cyc/mRad)	0.75mRad MTF
Δx	0.75 mRad	0.00	1.00
Δy	0.75 mRad	0.25	0.78
		0.50	0.55
		0.75	0.35
		1.00	0.15
		1.10	0.085
		1.25	0.02
		1.30	0.00
		2.00	0.00
		2.50	0.00
		3.00	0.00

Shumaker [Ref. 8, p. 8-52] shows a recalculation of the system MTF and MRT for a decrease of optical magnification, increasing the detector angular subtense to 1 mRad. This was taken as a guide in deducing the comparison with Figure 13. An additional check point is the expectation of the asymptotic behavior of the MRT(v) at a critical spatial frequency between $0.7/\Delta x$ and $0.9/\Delta x$. The 1.0 mRad and 0.25 mRad curves in Figure 13 show the MTF versus spatial frequency for the example system with NFOV and WFOV. The cutoff behavior of the MTF gives an indication of the limiting behavior of MRT. The estimated MTF (WFOV) is shown in Figure 13 compared with the NFOV and Shumaker's 1 mRad model.

For our comparison MRT, a modification of Shumaker's MTF computation was made with the results shown in Figure 13. The comparison curve lies between the curves for the Narrow and Wide Shumaker's example cases, as expected, with a cutoff very close to 1.3 cyc/mRad as appropriate for $\Delta x = 0.75$ mRad.

VI. DATA COMPUTATIONS AND ANALYSIS

The process of comparison can be outlined as follows :

1. The target ship signature T_s was obtained from thermal images obtained with the airborne AGA operated by NRaD and compensated to zero range by Hughes and McGrath .[Ref. 11]

2. Ship temperature and sea background temperature were converted to in-band radiance by application of Planck function.

3. SEARAD transmission code was used to calculate path transmittance and path radiance for the path from the target to the detection /recognition point as reported by the operational FLIR operators.

4. Ship and background radiance were corrected to the detection/recognition range using the SEARAD outputs.

5. Ship and background radiance at detection point were converted to apparent temperature using the inverse Planck function.

6. Apparent temperature difference ΔT_{app} at maximum range was compared with the postulated MRTD or MDTD respectively calculated for the same target-sensor locations. If the criteria for detection or recognition are correct, and the MRTD and MDTD data are appropriate, the apparent temperature difference should match the MRTD or MDTD.

An example of the computation process is shown in the following section. The calculated results of the eight runs for ΔT and MDTD/MRTD as well as line pairs requirement for MRTD criterion at detection range are summarized in Table 10, Table 11, Table 12 and Table 13 respectively. The flow charts for the calculation of ΔT_{app}, MDTD/MRTD and line pairs requirement at detection range are outlined in Figure 6, Figure 7, Figure 8 and Figure 9 respectively.

A.   DATA COMPUTATION STEPS

Run 1, Detection Time : August 04, 04:11(Zulu), 1992

1. Apparent ΔT Computation

- **Step 1,** The data for ship temperature T_s corrected to zero range is taken from the Table of Appendix C of Hughes and McGrath [Ref. 11] and is reproduced here in Table 2 for reference. The average of six ship temperature measurements at port aspect is 288.3 ^{0}K. The average ship temperature for each aspect is shown in Table 9.

- **Step 2,** The ship temperature is then converted to in-band radiance N_s at zero range

$$N_s = \frac{\varepsilon \sigma T^4}{\pi} \Delta q =$$

$$0.95 \times 5.67 \times 10^{-8} \times (288.3)^4 \times \frac{0.253578}{\pi} = 30.0 \,(W / m^2 Sr)$$

where

$\varepsilon = 0.95,$ emissivity of R / V POINT SUR.

$\lambda_1 T = 8\mu \times 288.3 = 0.23cm \times K \Rightarrow q1 = 1.2227 \times 10^{-1}$ (Radiation Table)

$\lambda_2 T = 12\mu \times 288.3 = 0.35cm \times K \Rightarrow q2 = 3.7585 \times 10^{-1}$ (Radiation Table)

$\Delta q = q2 - q1 = 2.53578 \times 10^{-1}$

The q values have 5 digits as reported in the radiation table (Appendix A) to keep the fraction of the radiant existence as close as possible to the integral of Planck's Law. The details of the Proportional Radiation technique are shown in Chapter II. [Ref. 5]

- **Step 3,** Run the SEARAD program to obtain transmittance τ and path radiance N_p between FLIR sensor and target. The inputs of the SEARAD code for the total 8 runs are tabulated in Appendix E and outputs of the SEARAD (transmittances, path radiances and background radiances) are shown in Table 6 (detection), Table 7 (classification) and Table 8 (identification) separately. In Run 1, the transmittance τ =0.0369 and path radiance N_p= 28.7 W/m²Sr.

- **Step 4,** Ship radiance N_{s+p} at full range $=N_s \tau + N_p$

$N_{s+p} = N_s \tau + N_p = 30.0 \times 0.0369 + 28.7 = 29.8$ (W / m² Sr)

- **Step 5,** Convert target radiance to equivalent blackbody temperature.
  In-band radiance at full range can be converted into equivalent blackbody temperature by use of Planck's radiation law using an interative computer

program and look-up table as shown in Appendix B. When $N_{s+p} =$ 29.8 W/m²Sr, the $T_{s+p} = 285.2$K.

- **Step 6**, From SEARAD output of step 3 , the background radiance N_b at full range is 29.6 W/m² Sr. By conversion with the computer program in Appendix B, the corresponding temperature is 284.8 K.

- **Step 7**, The apparent temperature difference at full range is then T_{s+p} -T_b =0.4 ^{0}C.

2. MDTD Computation at Detection Range

- **Step 1**, The projected area of the ship A_T on PORT aspect at detection range is shown in Figure 4.

$A_T = lw \sin \theta + hw \cos \theta \sin \phi + hl \cos \theta \cos \phi$

$= 41.5 \cdot 9.75 \cdot \sin(0.85) + 8.8 \cdot 9.75 \cdot \cos(0.85) \sin(0) + 41.5 \cdot 8.8 \cdot \cos(0.85) \cos(0)$

$= 371 \, m^2$

where

$l = 41.5$ m (ship length)

$w = 9.75$ m (ship width)

$h = 8.8$ m (ship height)

$\phi = 0.85$ ^{0} (elevation angle, $\sin^{-1}$ (altitude / R))

$\theta = 0^0$ (azimuth angle, port aspect)

- **Step 2,** The critical dimension D_c of the ship $= \sqrt{A_T} = 19.3$ m

- **Step 3,** For pure detection, number of bars $N = 1$

- **Step 4,** The physical dimension to be resolved is $\chi = D_c/N = 19.3/1 = 19.3 \, m$

- **Step 5,** Target angular subtense $TAS = 10^6 \times A_T / R^2 = 10^6 \times 371 / (21000)^2 = 0.84 \, (mRad^2)$

- **Step 6,** The typical MDTD curve as a function of Target Angular Subtense (TAS) for Shumaker application that is applicable for WFOV is shown in Figure 12. From Figure 12 when $TAS = 0.8 \, mRad^2$, the corresponding $MDTD = 0.2^0 C$

31

3. MRTD Computation

a. MRTD for Classification

The observed classification range in Run 1 is 8000 m at elevation angle θ =2.2^0 and azimuth angle ϕ =0^0.

- **Step 1**, For this aspect, the target area is given by

$$A_T = lw \sin\theta + hw \cos\theta \sin\phi + hl \cos\theta \cos\phi$$

$$= 41.5 \cdot 9.75 \cdot \sin(2.2) + 8.8 \cdot 9.75 \cdot \cos(2.2) \sin(0) + 41.5 \cdot 8.8 \cdot \cos(2.2) \cos(0)$$

$$= 380 \ m^2$$

where

l = 41.5 m (ship length)

w = 9.75 m (ship width)

h = 8.8 m (ship height)

θ = 2.180 ^{0} (elevation angle, $\sin^{-1}$ (altitude / R))

ϕ = 0^0 (azimuth angle, port aspect)

- **Step 2**, The critical dimension of the ship $D_c = \sqrt{A_T} = 19.5$ m

- **Step 3**, From the Johnson Criterion, the number of bars N necessary to classify the ship is 4 cyc × 2 bars/cyc = 8 bars.

- **Step 4**, The physical dimension to be resolved is $\chi = D_c/N = 19.5/8 = 2.4$ m

- **Step 5**, The spatial frequency f_c characterizing the ship at classification range is:

$$f_c = \frac{R}{2000\chi} = \frac{8000}{2000 \cdot 2.4} = 1.7 \ (\text{cyc} / \text{m Rad})$$

- **Step 6**, The MRTD curve as a function of spatial frequency in WFOV for Common Module FLIR has been deduced in Chapter V and is shown in Figure 11. From Figure 11, the asymptotic behavior occurs at spatial frequency equals 1.33 cyc/mRad. When f_c=1.7 cyc/mRad, the MRTD can not be resolved, which indicates that using WFOV is inappropriate in this classification application.

b. *MRTD for Identification :*

The observed identification range in Run 1 is 6000 m at elevation angle $\theta = 2.8°$ and azimuth angle $\phi = 0°$

- **Step 1**, The projected area of the ship on PORT aspect for identification is:

$$A_T = lw \sin\theta + hw \cos\theta \sin\phi + hl \cos\theta \cos\phi$$
$$= 41.5 \cdot 9.75 \cdot \sin(2.8) + 8.8 \cdot 9.75 \cdot \cos(2.8)\sin(0) + 41.5 \cdot 8.8 \cdot \cos(2.8)\cos(0)$$
$$= 384 \ m^2$$

where

$l = 41.5$ m (ship length)

$w = 9.75$ m (ship width)

$h = 8.8$ m (ship height)

$\theta = 2.8°$ (elevation angle, $\sin^{-1}$ (altitude / R))

$\phi = 0°$ (azimuth angle, port aspect)

- **Step 2**, The critical dimension of the ship $D_c = \sqrt{A_T} = 19.6$ m

- **Step 3**, From the Johnson Criterion to classify ships, number of bars N necessary to classify the ship is 6.4cyc x 2 bar/cyc = 12.8 bars.

- **Step 4**, The physical dimension to be resolved is $\chi = D_c/N = 19.6/12.8 = 1.5$ m

- **Step 5**, The spatial frequency f_c characterizing the ship at identification range is $f_c = 6000/(2000\times1.5) = 2.0$ cyc/mRad

- **Step 6**, From Figure 11, when $f_c = 2.0$ cyc/mRad, the corresponding MRTD can not be resolved. This may show that using WFOV in this identification application is also inappropriate.

B.   LINE PAIRS REQUIREMENT AT DETECTION RANGE

In Run 1, the calculated apparent temperature difference ΔT_{app} at detection range is 0.4 °C. When the target can be resolved at this range, the ΔT_{app} must equal MRTD, namely MRTD = 0.4 °C. From Figure 11 we know that for WFOV, when MRTD = 0.4

°C, the corresponding critical spatial frequency to resolve the target equals 0.9 cyc/mRad.

From Equation (13) the critical spatial frequency $f_c = \dfrac{R}{2000\chi}$ = 0.9 cyc/mRad. At the detection range, R = 21000 m, the corresponding number of bars N necessary to resolve the target is D_c/χ= 1.65 bars, where D_c in Run 1 is 19.3 m. Therefore the line pairs require to resolve the target is half of the bars which is 0.83 cycles.

VII. RESULTS AND DATA ANALYSIS

The calculated apparent temperature difference ΔT, MDTD and MRTD for the experiment are shown in Table 10, Table 11 and Table 12 separately. Line pairs requirements to resolve the target at the detection range are shown in Table 13. Data were taken during the eight overflights in the period 04:11 to 05:22 (GMT) on August, 1992. The first four overflights were flown at approximately 300 m altitude, each pass at a different quadrant of the ship. The other four overflights were flown at about 150 m altitude. There were three runs approaching the PORT aspect, three runs approaching the starboard (STBD) aspect, one run approaching stern (STN) and one run approaching BOW aspect. The required meteorological data (including radiosonde measurement) for SEARAD code inputs were taken from the meteorological data that were recorded during the experiment, and are shown in Table 3 , Table 4 and Table 5. These meteorological data were the closest to the aircraft overflights. Ship (R/V POINT SUR) temperature was the average ship temperature taken from the AGA scene corrected for atmospheric effects for each aspect (PORT, STBD, STN and BOW). These data were extracted from Hughes and McGrath. [Ref. 11] Due to aircraft and balloon flight limitations around the R/V POINT SUR, there was at least two hours time difference between the apparent ship temperature measurements from the airborne AGA scene and the navy aircraft overflights. During the eight overflights, there was no great change in the atmospheric conditions.

The estimated MRTD curve and MDTD curve for calculating MRTD and MDTD at different ranges were derived from Shumaker's example 8-13 and 8-16 for a generic FLIR system in WFOV. The detector angular subtenses Δx and Δy were chosen as 0.75 mRad to represent a typical FLIR system in WFOV. The NET was chosen as 0.125 K, between 0.1 K to 0.25 K, due to degradation of the FLIR sensor after being in service for several years.

In SEARAD, the meteorological data inputs include wind speed (W_s), wind direction (W_D), visibility (VIS), and air mass character (AM). They also include the sea

temperature, aircraft altitude and viewing angle. For analysis purposes, the meteorological data were assumed to be the same for each run except for wind speed and wind direction. The outputs of SEARAD (atmospheric transmittance τ and path radiance N_P) at detection range, classification range and identification range are shown in Table 10, Table 11 and Table 12 separately. Comparisons for each range prediction are shown in the following four sections.

A.   DETECTION RANGE COMPARISON

Table 10 shows Apparent Temperature Difference ΔT_{app} at the observed detection range compared with the MDTD estimated for the postulated system at the same range. The data show very large scatter; the variation in the Temperature Difference is much more than that of the MDTD for observed ranges from 13 to 22 kilometers. The range of discrepancy is from 5 % to 600 % over this small data set. The data used include five angles of approach to the target and hence combinations of target temperature and apparent size. Comparison between observations with similar aspect, for example runs 5 with 7 at STBD aspect and 6 with 8 at PORT, show much better internal agreement due to approximately the same altitude and viewing angle; However run 2 at 70° azimuth shows very poor agreement.

B.   CLASSIFICATION RANGE COMPARISON

Table 11 shows Apparent Temperature Difference and characteristic target Spatial Frequency (f_c = Range/(2000 x critical resolution length), see section VI A.3, p.32) at the reported classification range. The values shown as MRTD are the values of the postulated system WFOV MRTD evaluated at the critical spatial frequency for classification, taken as 4 line pairs per critical dimension. The x entries on the MRTD row indicate that the WFOV MRTD cannot be evaluated at the required spatial frequency, since this falls beyond the asymptotic value. Although the range measurements were all reported to be made in WFOV, the comparison suggests that the observed ranges are

more appropriate to NFOV operation. The major uncertainty in this table may be the FLIR operator's decision that the target was in classification range. In the cases for which .comparison is possible, the apparent ΔT considerably exceeds the postulated wide field MRTD.

C. RECOGNITION RANGE COMPARISON

Table 12 shows Apparent Temperature Difference and characteristic target spatial frequency ($f_c =$ Range / 2000 x critical resolution length) at the reported identification range. The MRTD values are the values of the postulated system in WFOV. The MRTD was estimated at the critical spatial frequency for identification, taken as 6.4 line pairs per critical dimension. The x entries on the MRTD row, as in Table 11, indicate that the WFOV MRTD cannot be evaluated at the required spatial frequency. Although the range measurements were all reported to be made in WFOV, this comparison still suggests that the observed ranges are more appropriate to NFOV operation. The major uncertainty in this table may be due to the FLIR operator's subjective decision that the target was in identification range. Again, where comparison is possible, the apparent ΔT considerably exceeds the postulated WFOV MRTD.

D. RESOLUTION LINE PAIRS AT DETECTION RANGE

The Johnson Criterion for detection is stated as a required number of resolvable line pairs on the critical dimension of the target image. This can be compared with the estimated actual line-pairs at the detection range by setting the ΔT at this range equal to MRTD, and evaluating the corresponding spatial frequency. This comparison is shown in Table 13. The required line-pair number is seen to vary from 0.5 to 1.1, compared with the Johnson Criterion of 1. The spatial frequency values are read from the MRTD WFOV curve for the postulated system, shown in Figure 11.

37

E. DISCUSSION OF THE DATA

The comparisons of Table 11 through 13 show poor agreement between the MDTD/MRTD estimated for the postulated FLIR and the computed target-background temperature difference at the appropriate maximum range. No clear systematic relationship is apparent between these two quantities, and larger random deviations are present. A number of sources can be suggested for the discrepancies.

The time difference between the apparent ship signature measurement from AGA scene with the aircraft overflights measurement may cause some deviation of the calculated results.

The SEARAD code itself, if the inputs were selected properly, should agree to within a few degree Celsius with actual sea radiance in the long wave band (8 to 12μm). The results of the SEARAD output (τ and N_p) and the selection of input parameters may also cause the deviation of the computed ΔT_{app}.

The aircrew plays an important role during the measurement. The operator generally may not know exactly the target's characteristics. His primary experience is visual (0.4 to 0.7 μm). He can only state if the image on the screen resembles a visual scene. In this experiment, the aircrew recorded the detection range when he first saw a dot on the FLIR display screen. However, MRTD is a measurement of the performance of the entire system which includes the operator, so the measurements of classification and identification are subjective, a human interpretation of the displayed information. From the data collected by the aircrew in Table 3, the detection ranges for STBD aspect (run 2, 5 and 7) under similar conditions are 15000 m, 22000 m and 22000 m. The results for run 5 and run 7 match well with each other, but show great discrepancy with run 2. This discrepancy may be due to the different operators' perception.

The apparent temperature difference ΔT_{app} is a function of the FLIR sensor altitude and viewing angle. During some overflights, the sensor altitude and viewing angle changed slightly. For example, in run5 and run 7, the sensor altitude was 140 m and 160 m with viewing angle 0.36° and 0.43 °, which shows almost the same geometry. The comparison

of ΔT_{app} with MDTD in Table 10 at STBD aspect show agreement between runs. This is also found for run 6 and run 8 at PORT aspect.

Field of view is also an important consideration for FLIR performance. In normal operation a wide field of view (WFOV) is initially used to provide situational awareness to the operator, but after the target is detected the operator switches to a narrow field of view (NFOV). During the eight runs in this data set the aircrew reportedly always used the WFOV for detection, classification and identification ranges. The results for detection shown in Table 10 indicate moderate agreement, but show large discrepancy for MRTD at classification and recognition range, as shown in Table 11 and Table 12. The data appear more consistent with NFOV measurement. A comparison with the NFOV MRTD might show closer agreement.

Lastly, the " postulated" FLIR model MDTD and MRTD are based on some relatively broad assumptions. The calculated values at detection, classification and identification ranges for varies target area and range and meteorological conditions show a considerable level of internal consistency, leading to a modest level of confidence in the model.

VIII. CONCLUSIONS

The main goals of this thesis were to evaluate the followings :

• apparent target-background temperature difference (ΔT_{app}) at maximum range.

• MDTD/MRTD of a typical FLIR system applied to PREOS92 experiment.

• line pairs requirement at detection range to resolve the target.

In the calculation procedures, the theoretical Planck's radiation law was applied to find ΔT_{app}. The propagation code (SEARAD) provided the atmospheric transmittance and path radiance. Measured atmospheric parameters were selected as close in time to the operational aircraft overflights as possible using PREOS 92 data as inputs to the SEARAD code. The ship was required as a rectangular parallelepiped model of the ship's physical length, width and height for MDTD/MRTD evaluation. The geometry data for MDTD/MRTD evaluations were also selected from the PREOS 92 experiment measurement data. The MDTD/MRTD functions for a generic FLIR in wide field of view (WFOV) application were deduced following Shumaker. The Johnson criterion for the number of line pairs on a target was employed as a detection criterion and compared to the estimated line pairs computed from the data.

Based on the measured ranges reported in PREOS92 experiment and the calculated ΔT_{app} at different ranges, the ΔT_{app} at the detection range matches better with MDTD using the same sensor altitude and viewing angle. However, the measured ranges reported are all subjective due to the operator's interpretation of the displayed information, thus the final results of this calculation are all estimations. Furthermore, the calculated MRTD in Table 10, Table 11 and Table 12 show that the most of the required spatial frequencies for the ranges found in this experiment are higher than the WFOV cutoff spatial frequency (1.3 cyc/mRad) , therefore the target should not have been resolved. This suggests that using NFOV in this experiment for target classification and identification would be more appropriate.

Additionally, the calculated line pairs needed at the detection range for MRTD criterion show that there is 10% ~50 % error range for the 8 runs. Compared to the Johnson Criterion quoted as 1 ± 0.25 mRad, this error is acceptable for the calculation procedure based on the MRTD curve derived from a theoretical equation used in WFOV. This MRTD curve is only a typical curve that is considered to be suitable for this application.

Since only 8 runs that have been applied in this thesis, more runs should improve the comparison.

SKY
RADIANCE

SHIP + PATH RADIANCE

REFLECTED SKY + PATH +
SEA-SURFACE RADIANCE
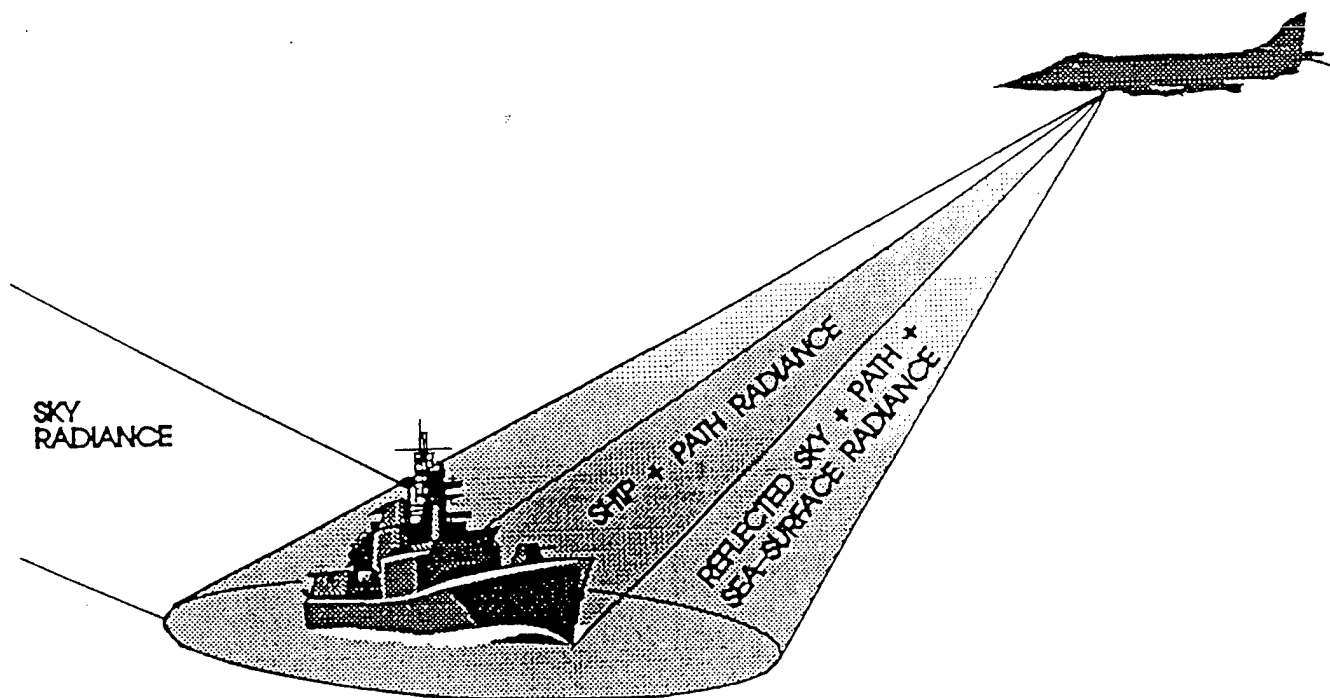
Figure 1. Scenario for Detecting a Ship with an Airborne FLIR Sensor
From [Ref. 2, p. 3]

42
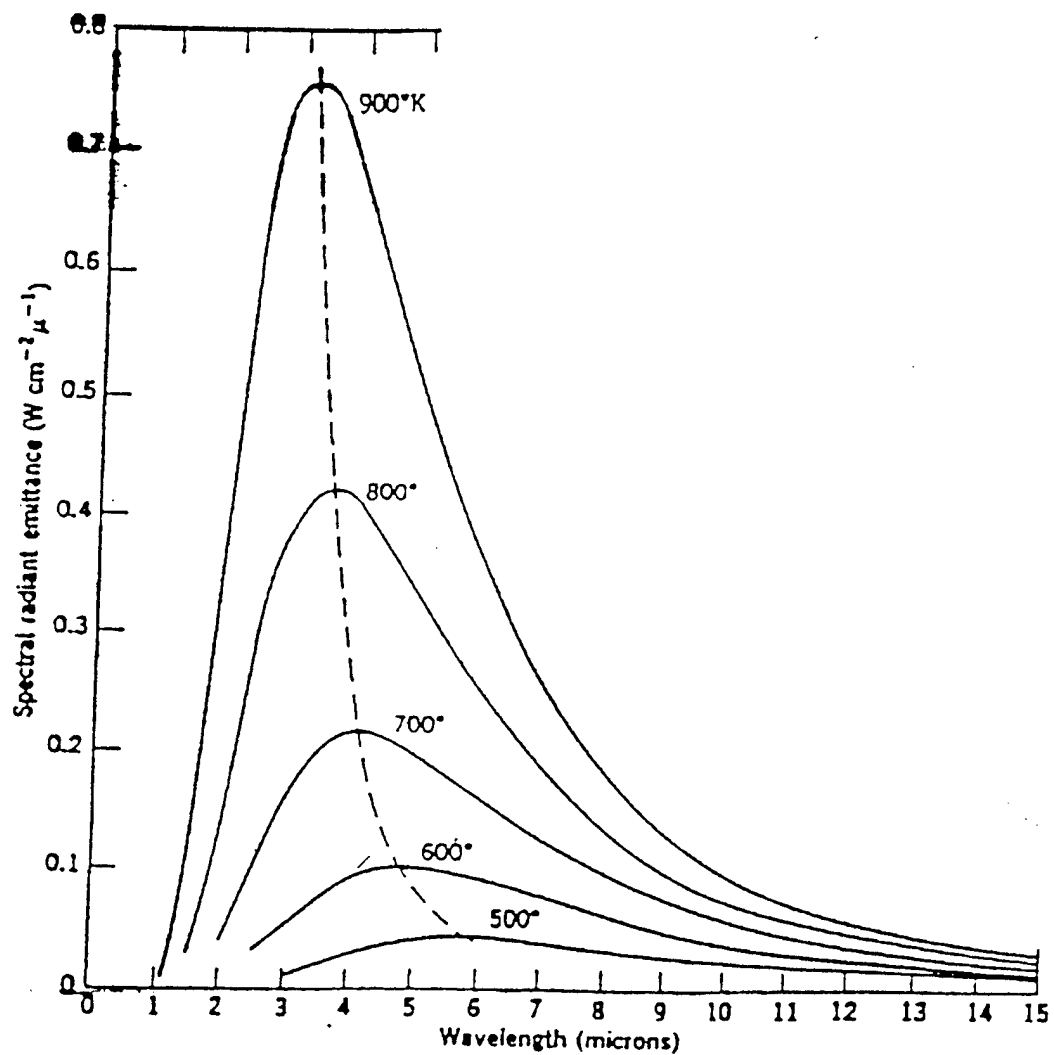
Figure 2. Spectral Radiant Emittance of a Blackbody Ranging from 500 to 900 K
From [Ref. 5, p. 55]

43
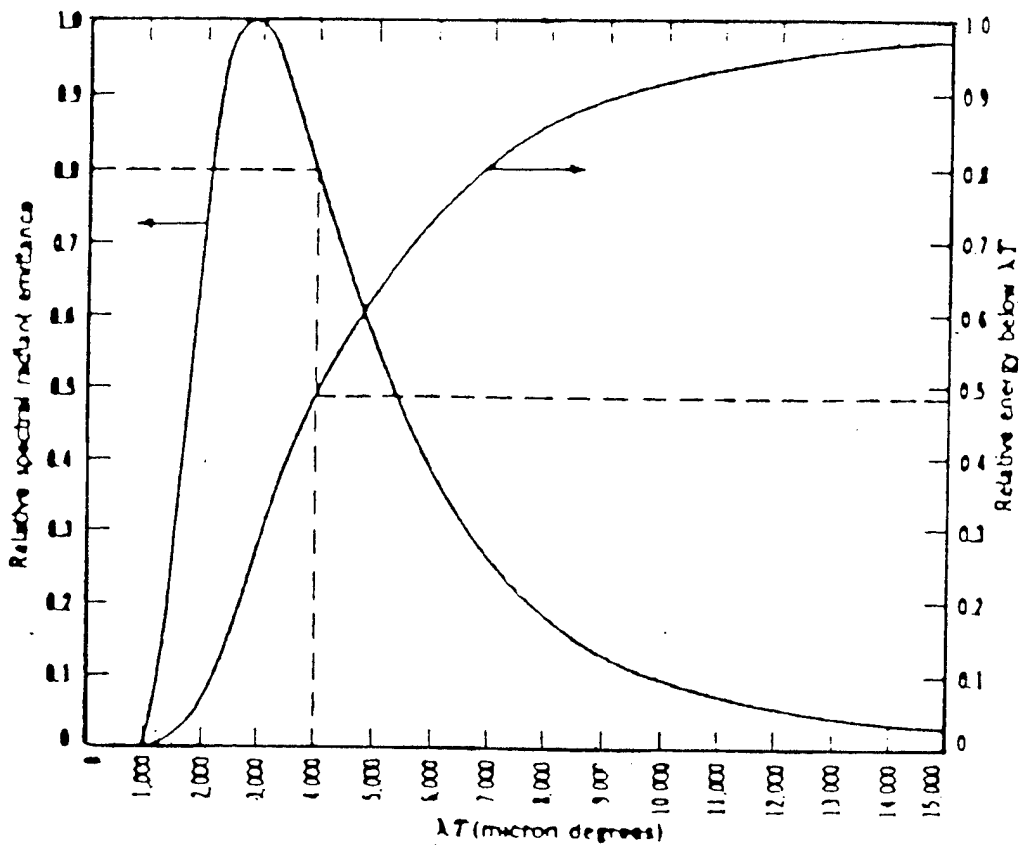
Figure 3. Universal Blackbody Curve
From [Ref. 5]

44
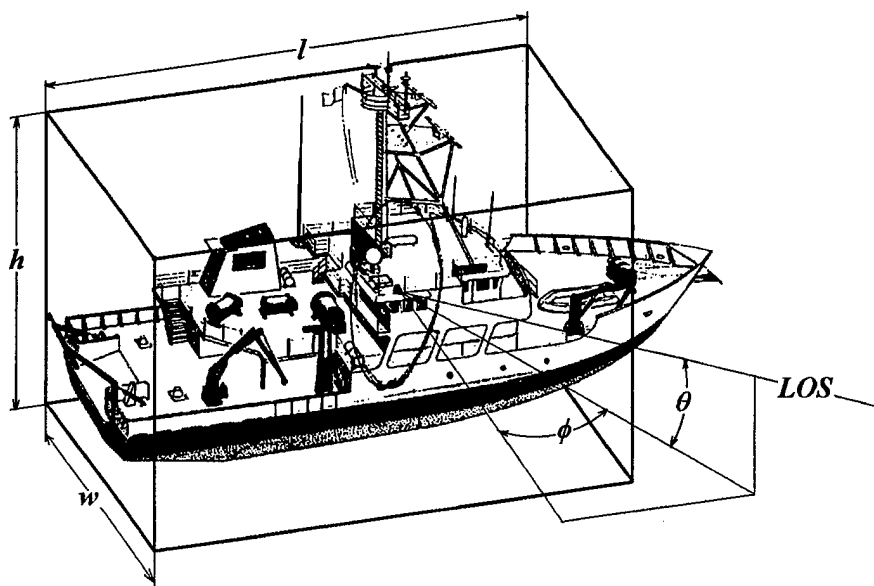
Figure 4. Orientation of Ship Target Model

$$f_c = \frac{R}{2000\,\chi} \quad (\text{Cyc/mRad})$$

$$\chi = \frac{D_c}{N}$$
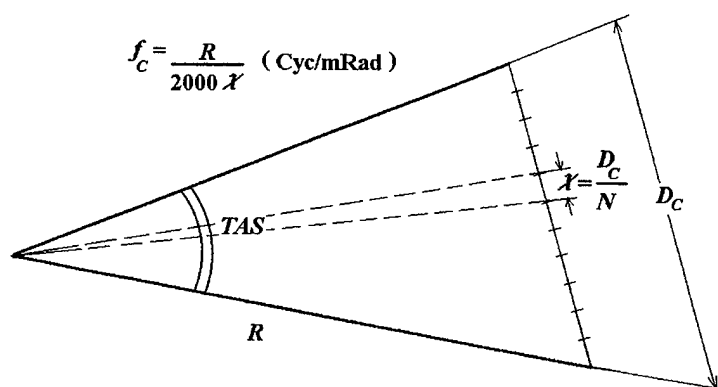
N = Number of Bars in the Bar Chart
R = Slant Range
TAS = Target Angular Subtense
D_c = Critical Dimension
χ = Physical Dimension to be Resolved
f_c = Spatial Frequency of Bar

Figure 5. Relation Between Spatial Frequency, Range R and Physical Dimension χ

Figure 6. ΔT Computation Flow Chart
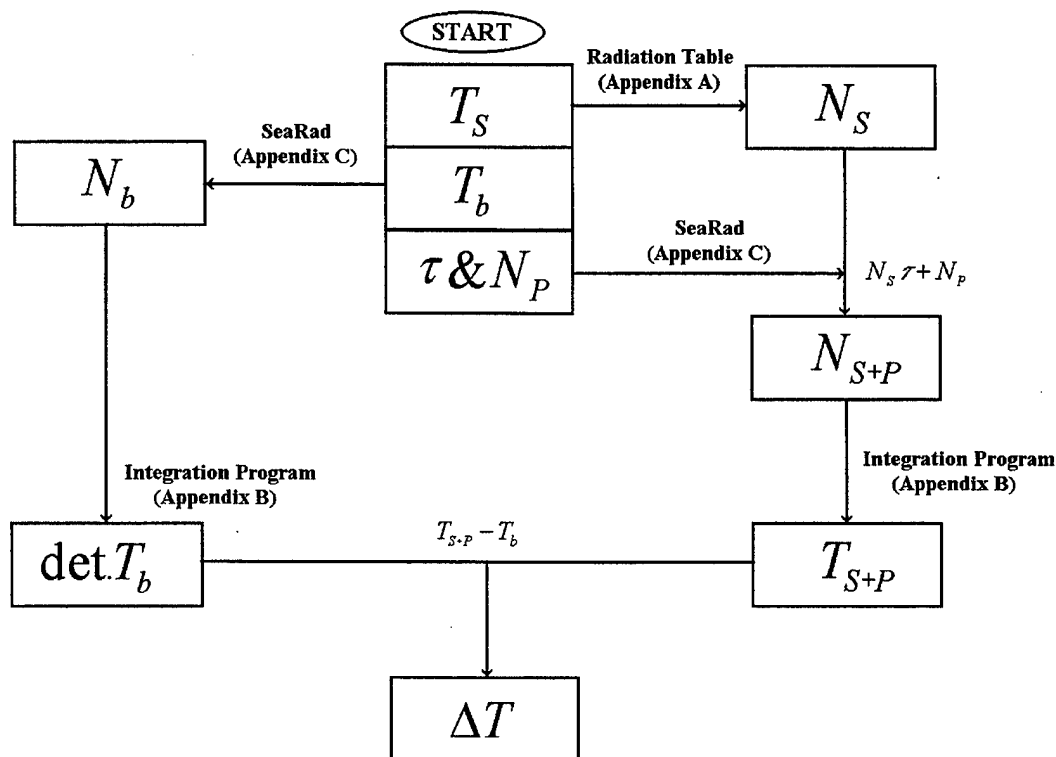
T_s = Ship Temperature at Zero Range

T_b = Sea Temperature at Zero Range

τ = Transmittance

N_p = Path Radiance

N_b = Background Radiance

$\det T_b$ = Background Temperature at Detection Range

N_s = Ship Radiance at Zero Range

N_{s+p} = Ship Radiance at Detection Range

T_{s+p} = Ship Temperature at Detection Range

START

A_T

TAS $\dfrac{10^6 A_T}{R^2}$

Figure 12

$MDTD = f(TAS)$
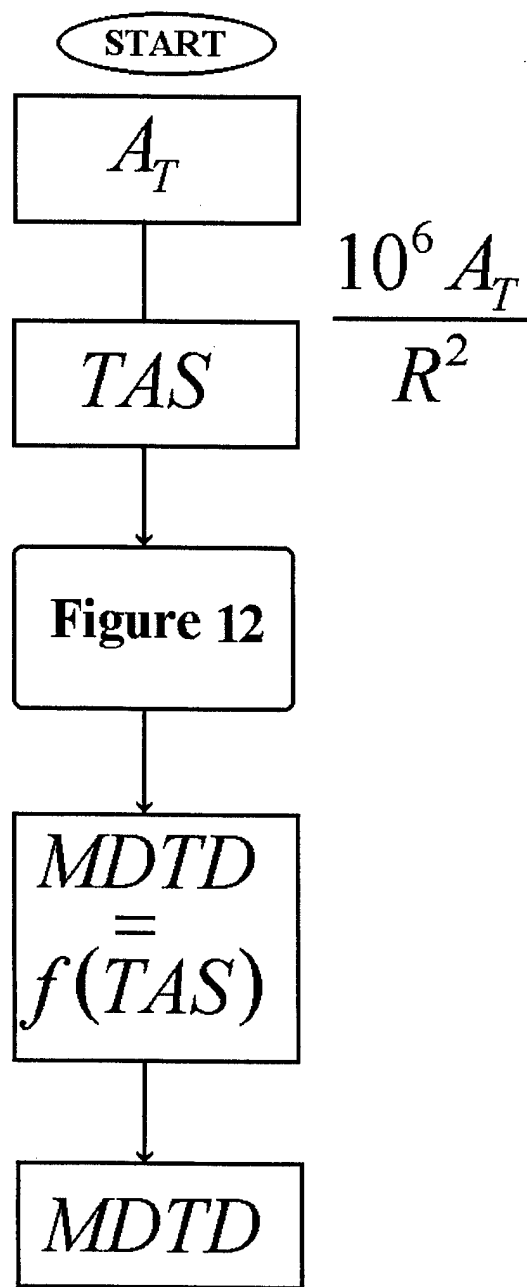
$MDTD$

TAS = Target Angular Subtense

Figure 7. MDTD Determination Flow Chart

START

$$A_T$$

$$\sqrt{A_T}$$

$$D_C$$

A_T = Projected Area of the Target

D_C = Critical Dimension of the Target

f_C = Critical spatial frequency

$L.P.$= Line pairs required
to resolve the target

Johnson Criterion:

$$L.P.= 4(\text{Classify})$$

$$L.P.=6.4(\text{Identify})$$

$$\frac{D_C}{N}$$

$$\chi$$

$$f_C = \frac{R}{2000\,\chi}$$

$$f_C$$
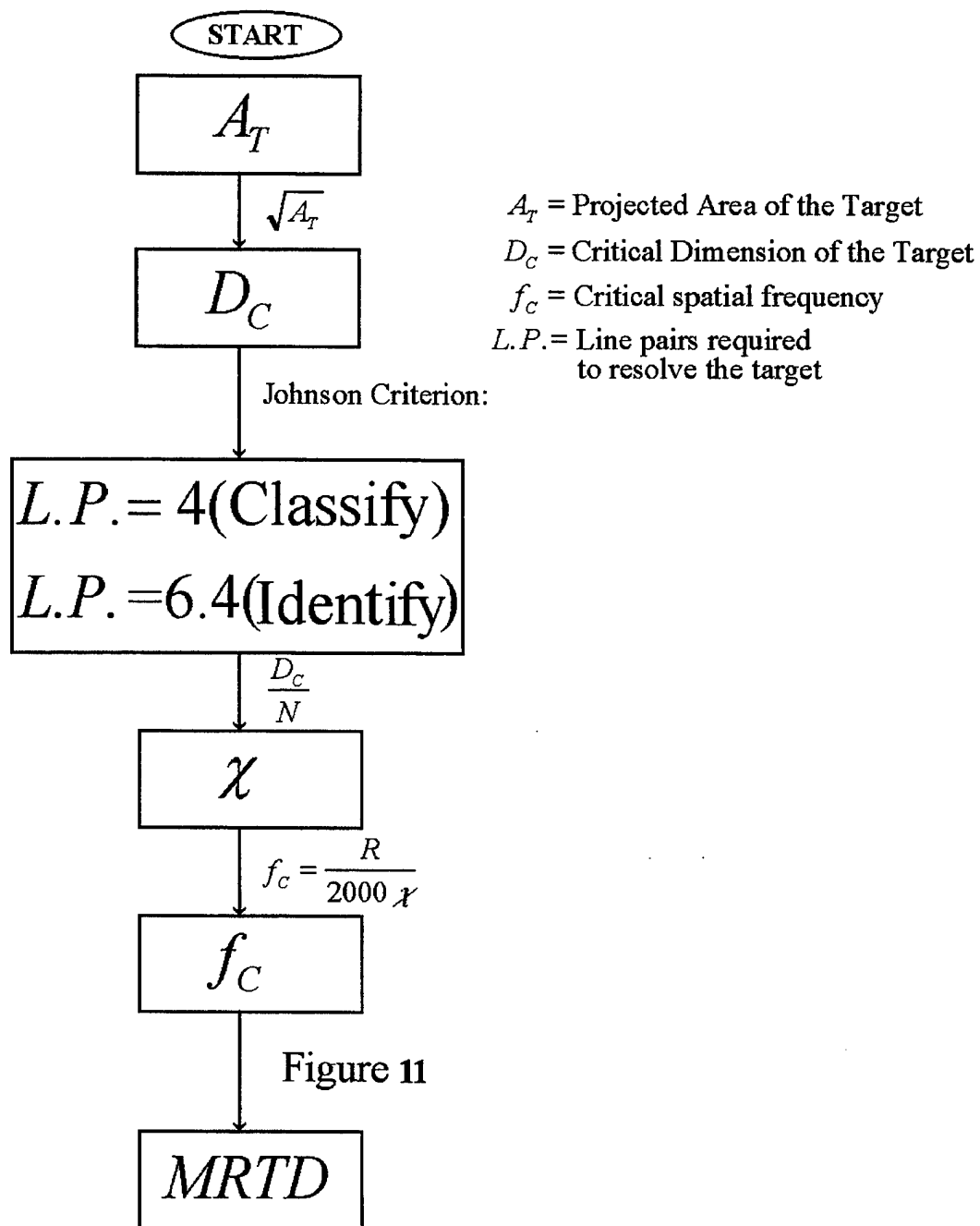
Figure 11

$$MRTD$$

Figure 8. MRTD Determination Flow Chart

48

START

A_T

$\sqrt{A_T}$

D_C

$f_C = \dfrac{R}{2000\dfrac{D_C}{N}}$

N

$2N$

$L.P.$

A_T = Projected Area of the Target

D_C = Critical Dimension of the Target

f_C = Critical spatial frequency

N = Number of bars to be resolved

$L.P.$ = Line pairs required
to resolve the target
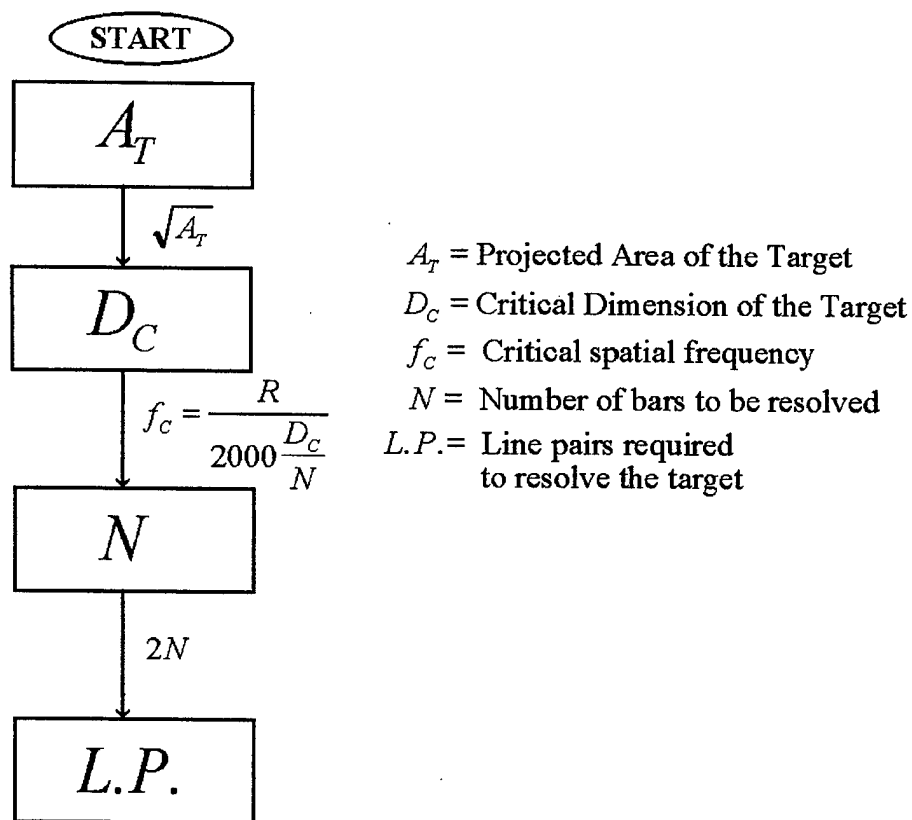
Figure 9. Line Pairs Calculation Flow Chart
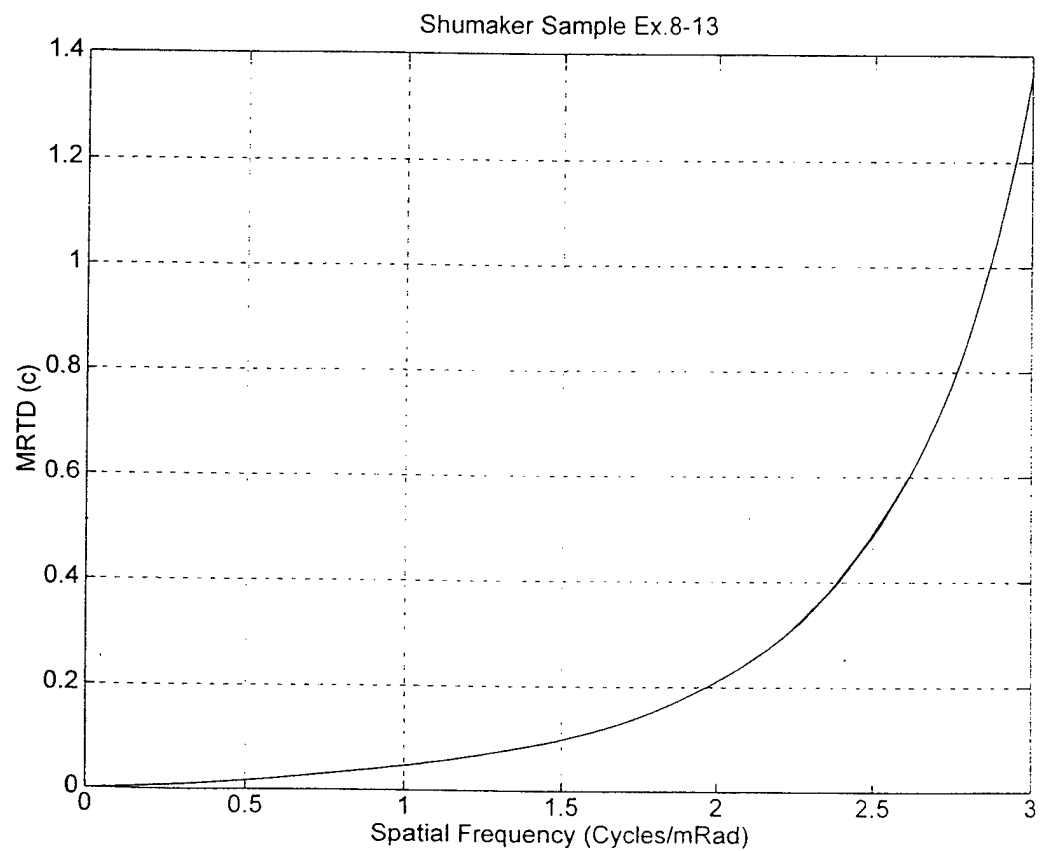
Figure 10.   MRTD Sample System in NFOV
From [Ref. 8]

MRTD as a function of Spatial Frequency in WFOV

1. NET=0.125 C

2. Dx=0.75 mrad. Dy=0.75 mrad

3. MRT WFOV
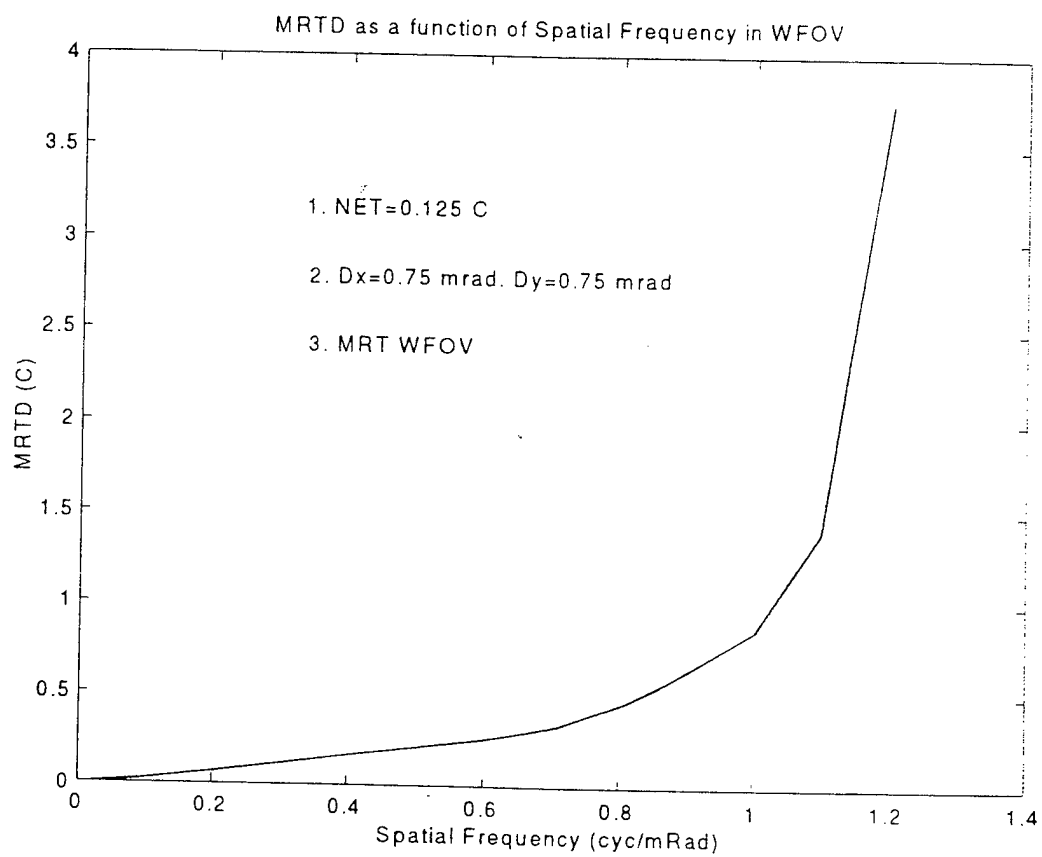
Figure 11. MRTD as a Function of Spatial Frequency (WFOV)

51

MDTD versus TAS Plot in WFOV

1. NET=0.125 C

2. Detector Subtense dx=dy=0.75 mRad

3. Detector Resolution rD=dx=0.75 mRad

(WFOV)

MDTD (C)

Target Angular Subtense (mRad)^2
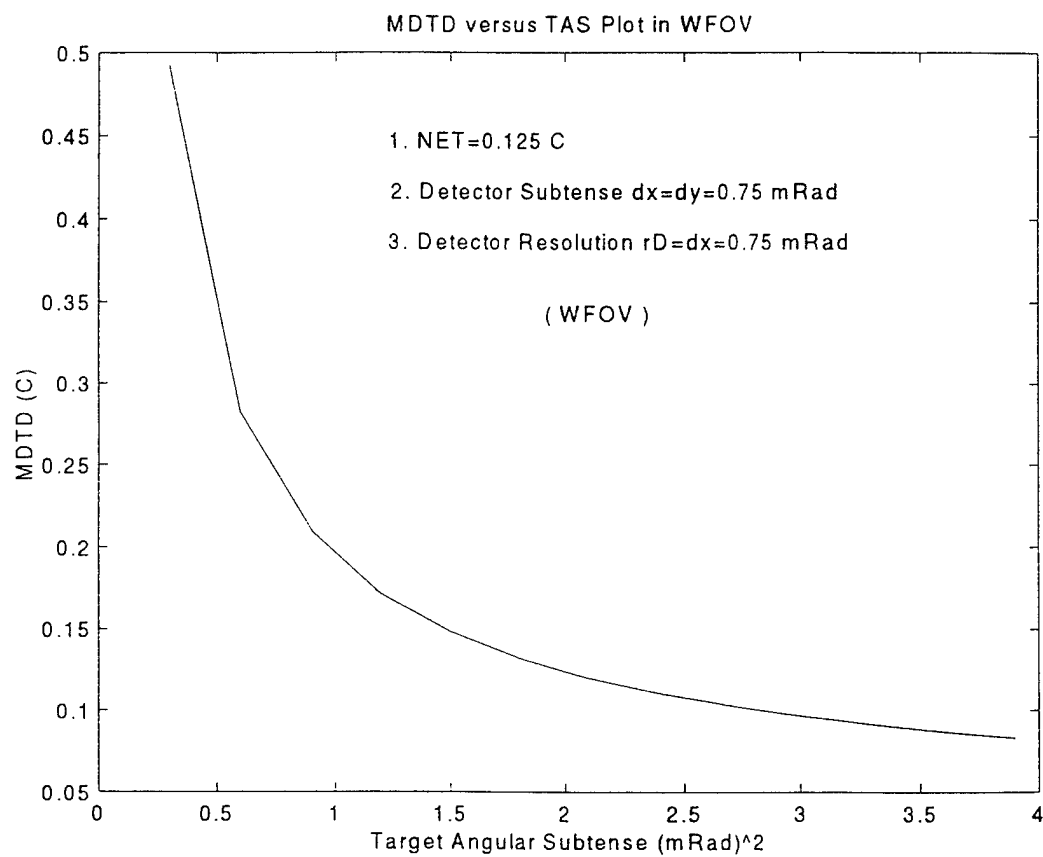
Figure 12. MDTD as a Function of Target Angular Subtense (WFOV)

52

MTF as a Function of Spatial Frequency
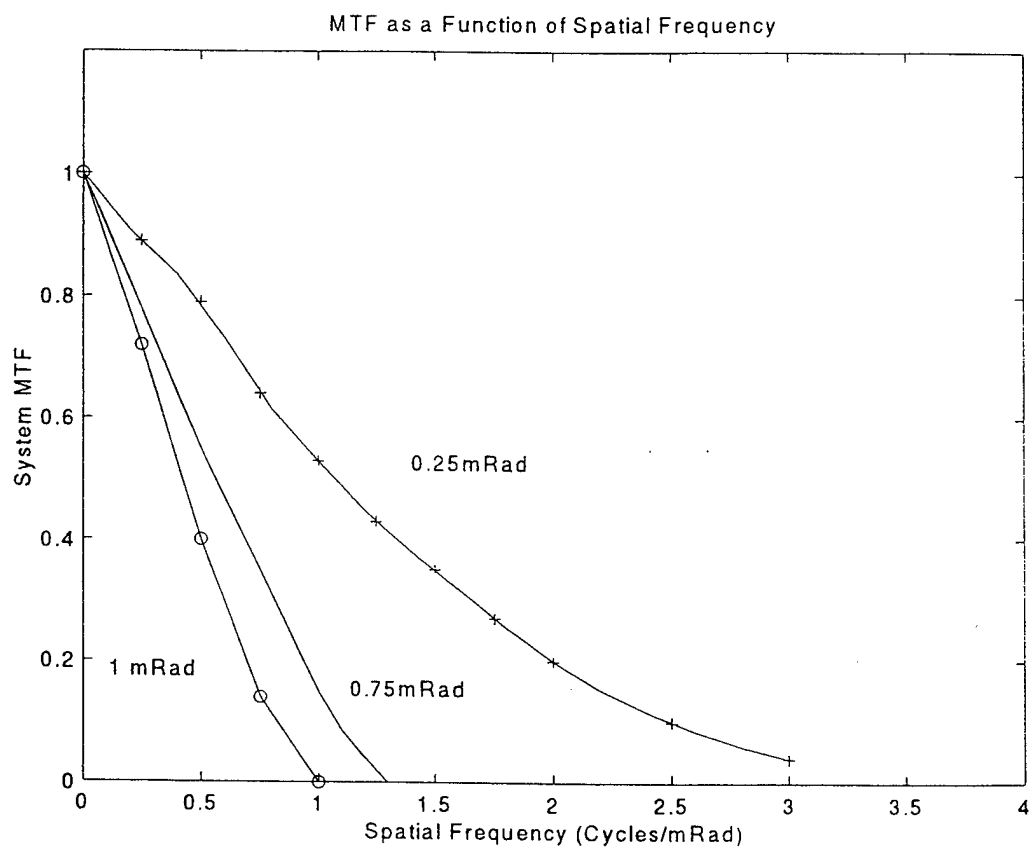
Figure 13. Comparison of System MTF in WFOV and NFOV

Table 1. Johnson Criterion

Discrimination Level	Cycles Across Minimum Dimension
Detection	1.0
Recognition	4.0
Identification	6.4

Table 2. Ship Temperature Corrected To Zero Range
From Thermal Images
After[Ref. 11]

Date	Time (GMT)	AGA Scene	T(ship) ^{0}C
8/04	01:37:45	PORT	14.83
	01:37:47	PORT	14.56
	01:39:55	STBD	15.06
	01:39:57	STBD	15.17
	01:40:01	STBD	15.57
	01:46:18	STBD	16.68
	01:46:20	STBD	17.13
	01:47:49	PORT	15.72
	01:47:51	PORT	15.97
	01:54:49	STN	16.70
	01:56:37	STBD	15.72
	01:59:35	STBD	15.52
	01:59:37	STBD	15.97
	02:00:16	STN	16.91
	02:00:51	PORT	15.77
	02:01:31	BOW	14.79
	02:02:08	STBD	16.21
	02:05:50	BOW	14.79
	02:06:37	STBD	17.19
	02:07:20	STN	17.82
	02:07:53	PORT	15.18
	02:08:22	BOW	14.99

Table 3. Data From Aircraft Overflights Measurements

Aircraft Run Numbers	1	2	3	4	5	6	7	8
Run Time (GMT)	04:11	04:25	04:32	04:41	04:49	05:03	05:11	05:22
Ship Aspect	PORT	STBD	STN	BOW	STBD	PORT	STBD	PORT
Aircraft Altitude (m)	313	307	310	309	139	155	164	162
Observed Detection Range (m)	21,000	15,000	13,000	15,000	22,000	15,000	22,000	15,000
Elevation Angle for Observed Detection Range (degree)	0.8	1.2	1.4	1.2	0.4	0.6	0.4	0.6
Observed Classification Range (m)	8,000	4,500	1,800	8,000	15,000	4,600	9,000	8,000
Elevation Angle for Observed Classification Range (degree)	2.2	3.8	9.8	2.2	0.5	1.9	1.0	1.1
Observed Recognition Range (m)	6,400	3,600	9000	3,600	3,600	2,700	3,600	5,500
Elevation Angle for Recognition Range (degree)	2.8	4.8	20.0	4.8	2.2	3.2	2.6	1.7

Table 4. Radiosonde measurement

4 August 1992 0401 (GMT)
29 layers

H(km)	P(mb)	T(C)	RH(%)	Sets Units for H,P,T,RH
0.007	1013.600	12.200	94.0	ABH
0.025	1011.625	12.280	92.4	ABH
0.050	1008.881	12.390	90.2	ABH
0.075	1005.709	12.499	88.0	ABH
0.120	1000.000	12.700	84.0	ABH
0.208	989.500	12.300	84.0	ABH
0.253	984.200	12.200	84.0	ABH
0.270	982.300	12.900	83.0	ABH
0.365	971.300	16.700	30.0	ABH
0.543	951.400	23.700	6.0	ABH
0.558	949.800	24.300	6.0	ABH
0.771	926.800	25.600	4.0	ABH
1.525	850.000	21.700	7.0	ABH
3.174	700.000	12.400	5.0	ABH
3.182	699.300	12.300	5.0	ABH
4.017	632.100	5.200	14.0	ABH
4.514	594.600	3.900	4.0	ABH
4.974	561.600	0.000	6.0	ABH
4.984	560.900	0.000	5.0	ABH
5.891	500.000	-6.700	7.0	ABH
6.295	474.700	-10.400	11.0	ABH
6.856	441.000	-13.700	6.0	ABH
6.880	439.600	-13.800	25.0	ABH
6.912	437.800	-14.100	8.0	ABH
7.590	400.000	-19.100	4.0	ABH
8.037	376.600	-21.800	5.0	ABH
8.184	369.100	-23.100	10.0	ABH
8.232	366.700	-23.500	36.0	ABH
8.284	364.100	-24.000	14.0	ABH

Table 5. Meteorological Data And Sea Temperatures For SEARAD Inputs

Aircraft Run Numbers	1	2	3	4	5	6	7	8
Run Time (GMT)	04:11	04:25	04:32	04:41	04:49	05:03	05:11	05:22
Air Mass Character	1.6	1.6	1.6	1.6	1.6	1.6	1.6	1.6
Visibility (VIS)	27.08	27.08	27.08	27.08	27.08	27.08	27.08	27.08
Wind Speed V_C (m/s)	10.19	11.68	12.12	13.26	12.04	8.28	8.05	7.94
Wind Direction V_D (degree)	298.911	289.438	283.893	275.374	277.645	295.427	289.911	293.928
Sea Temperature T_{sea} (°C)	11.7	11.7	11.7	11.7	11.7	11.7	11.7	11.7

Table 6. Atmospheric Transmittance (τ) And Path Radiance (N_p) for Detection Range From SEARAD Output File

Aircraft Run Numbers	1	2	3	4	5	6	7	8
Run Time (GMT)	04:11	04:25	04:32	04:41	04:49	05:03	05:11	05:22
Transmittance τ	0.0369	0.0977	0.130	0.0965	0.0092	0.0672	0.0150	0.0689
Path Radiance N_p (W/m²Sr)	28.7	26.8	25.8	26.8	29.3	27.7	29.2	27.6
Radiance at Observed Detection Range (w/m² Sr)	29.6	29.2	29.1	29.2	29.5	29.3	29.6	29.3
Ship Aspect	PORT	STBD	STN	BOW	STBD	PORT	STBD	PORT

Table 7. Atmospheric Transmittance (τ) and Path Radiance (Np) for Classification Range from SEARAD Output File

Aircraft Run Numbers	1	2	3	4	5	6	7	8
Run Time (GMT)	04:11	04:25	04:32	04:41	04:49	05:03	05:11	05:22
Transmittance τ	0.261	0.634	0.685	0.252	0.0726	0.428	0.208	0.241
Path Radiance N_P (W/m^{2}Sr)	21.9	10.6	9.0	22.0	27.4	16.8	23.5	22.5
Radiance at Observed Classification Range (W/m^2 Sr)	28..5	27.3	27.1	28.5	29.2	27.6	28.6	28.4
Ship Aspect	PORT	STBD	STN	BOW	STBD	PORT	STBD	PORT

Table 8. Atmospheric Transmittance (τ) and Path Radiance (Np) for Identification Range from SEARAD Output File

Aircraft Run Numbers	1	2	3	4	5	6	7	8
Run Time (GMT)	04:11	04:25	04:32	04:41	04:49	05:03	05:11	05:22
Transmittance τ	0.341	0.510	0.805	0.507	0.487	0.577	0.498	0.371
Path Radiance N_p (W/m^{2}Sr)	19.4	14.3	5.5	14.4	14.9	12.3	14.7	18.5
Background Radiance at Observed Identification Range (W/m^{2}Sr)	28.2	27.5	28.2	27.7	27.4	26.9	27.3	27.8
Ship Aspect	PORT	STBD	STN	BOW	STBD	PORT	STBD	PORT

Table 9. Average Ship Temperature (°C) for Each Measurement
After [Ref. 11]

Date	PORT	STBD	STN	BOW
04 August 92	15.3	16.0	17.2	15.1

Table 10. Comparison of Estimated MDTD with Calculated ΔT_{app} at Detection Range

Run	1	2	3	4	5	6	7	8
Observed Range (m)	21000	15000	13000	15000	22000	15000	22000	15000
Aspect	PORT	STBD	STN	BOW	STBD	PORT	STBD	PORT
ΔT_{app} (°C)	0.40	0.98	1.40	0.93	0.14	0.44	0.20	0.40
MDTD(°C)	0.23	0.20	0.20	0.27	0.21	0.14	0.21	0.14

Note : Run 2 is at 70° aspect angle

Table 11. Comparison of Estimated MRTD with Calculated ΔT_{app} at Classification Range

Run	1	2	3	4	5	6	7	8
Aspect	PORT	STBD	STN	BOW	STBD	PORT	STBD	PORT
Spatial Freq. (cyc/mRad)	1.7	1.2	0.6	3.3	3.0	0.9	1.9	1.7
ΔT_{app} (°C)	2.1	4.6	5.6	1.8	0.8	3.6	1.9	2.3
MRTD (°C)	×	3.4	0.2	×	×	0.6	×	×

Note : × indicates MRTD can not be calculated

Table 12. Comparison of Estimated MRTD with Calculated ΔT_{app} at Identification Range

Run	1	2	3	4	5	6	7	8
Aspect	PORT	STBD	STN	BOW	STBD	PORT	STBD	PORT
Spatial Freq. Cyc/mRad)	2.1	1.5	0.4	2.1	1.2	0.9	1.2	1.8
ΔT_{app} (°C)	2.6	4.1	3.9	2.2	3.9	4.9	4.6	3.3
MRTD (°C)	×	×	0.2	×	3.2	0.6	3.2	×

59

Table 13. Line Pairs Requirement at Detection Range For MRTD Criterion

Run		1	2	3	4	5	6	7	8
Aspect		PORT	STBD	STN	BOW	STBD	PORT	STBD	PORT
MRTD at Det. Range	f_C (cyc/mRad)	0.9	1.0	1.1	1.1	0.3	0.9	0.4	0.9
	Line Pairs (cycles)	0.8	1.0	0.8	0.7	0.5	1.1	0.5	1.1

Note : Spatial Frequency is taken from Figure 11 in WFOV

APPENDIX A. PROPORTIONAL RADIATION TABLE

From [Ref. 5]

The "Proportional Radiation", q=f(λ , T) represents the fraction of the radiant exitance which is emitted by a blackbody at temperature T at all wavelengths up to the selected values of λ . It is obtained from the integral over the Planck Law for wavelengths up to the selected values divided by the integral over all wavelengths, i.e.

$$q = \frac{\int_0^{\lambda} M(\lambda T)\, d\lambda}{\int_0^{\infty} M(\lambda T)\, d\lambda}$$

λ.T cm.K	q	λ.T cm.K	q	λ.T cm.K	q
0.050	$1.3652 \cdot 10^{-9}$	0.140	$7.9053 \cdot 10^{-3}$	0.460	$5.8057 \cdot 10^{-1}$
0.052	$3.6788 \cdot 10^{-9}$	0.150	$1.3023 \cdot 10^{-2}$	0.480	$6.0880 \cdot 10^{-1}$
0.054	$9.1749 \cdot 10^{-9}$	0.160	$1.9962 \cdot 10^{-2}$	0.500	$6.3494 \cdot 10^{-1}$
0.056	$2.1358 \cdot 10^{-8}$	0.170	$2.8858 \cdot 10^{-2}$	0.520	$6.5912 \cdot 10^{-1}$
0.058	$4.6745 \cdot 10^{-8}$	0.180	$3.9754 \cdot 10^{-2}$	0.540	$6.8146 \cdot 10^{-1}$
0.060	$9.6798 \cdot 10^{-8}$	0.190	$5.2613 \cdot 10^{-2}$	0.560	$7.0209 \cdot 10^{-1}$
0.062	$1.9069 \cdot 10^{-7}$	0.200	$6.7331 \cdot 10^{-2}$	0.580	$7.2116 \cdot 10^{-1}$
0.064	$3.5907 \cdot 10^{-7}$	0.210	$8.3750 \cdot 10^{-2}$	0.600	$7.3877 \cdot 10^{-1}$
0.066	$6.4902 \cdot 10^{-7}$	0.220	$1.0168 \cdot 10^{-1}$	0.620	$7.5505 \cdot 10^{-1}$
0.068	$1.1302 \cdot 10^{-6}$	0.230	$1.2091 \cdot 10^{-1}$	0.660	$7.8402 \cdot 10^{-1}$
0.070	$1.9025 \cdot 10^{-6}$	0.240	$1.4122 \cdot 10^{-1}$	0.700	$8.0885 \cdot 10^{-1}$
0.072	$3.1045 \cdot 10^{-6}$	0.250	$1.6239 \cdot 10^{-1}$	0.740	$8.3020 \cdot 10^{-1}$
0.074	$4.9236 \cdot 10^{-6}$	0.260	$1.8423 \cdot 10^{-1}$	0.780	$8.4861 \cdot 10^{-1}$
0.076	$7.6070 \cdot 10^{-6}$	0.270	$2.0653 \cdot 10^{-1}$	0.820	$8.6455 \cdot 10^{-1}$
0.078	$1.1473 \cdot 10^{-5}$	0.280	$2.2911 \cdot 10^{-1}$	0.860	$8.7840 \cdot 10^{-1}$
0.080	$1.6923 \cdot 10^{-5}$	0.290	$2.5183 \cdot 10^{-1}$	0.900	$8.9048 \cdot 10^{-1}$
0.082	$2.4453 \cdot 10^{-5}$	0.300	$2.7454 \cdot 10^{-1}$	0.940	$9.010f \cdot 10^{-1}$
0.084	$3.4668 \cdot 10^{-5}$	0.310	$2.9712 \cdot 10^{-1}$	0.980	$9.1033 \cdot 10^{-1}$
0.086	$4.8287 \cdot 10^{-5}$	0.320	$3.1947 \cdot 10^{-1}$	1.00	$9.1455 \cdot 10^{-1}$
0.088	$6.6159 \cdot 10^{-5}$	0.330	$3.4150 \cdot 10^{-1}$	1.10	$9.3217 \cdot 10^{-1}$
0.090	$8.9269 \cdot 10^{-5}$	0.340	$3.6314 \cdot 10^{-1}$	1.20	$9.4532 \cdot 10^{-1}$
0.092	$1.1874 \cdot 10^{-4}$	0.350	$3.8432 \cdot 10^{-1}$	1.30	$9.5331 \cdot 10^{-1}$
0.094	$1.5586 \cdot 10^{-4}$	0.360	$4.0502 \cdot 10^{-1}$	1.40	$9.6304 \cdot 10^{-1}$
0.096	$2.0204 \cdot 10^{-4}$	0.370	$4.2518 \cdot 10^{-1}$	1.50	$9.6909 \cdot 10^{-1}$
0.098	$2.5885 \cdot 10^{-4}$	0.380	$4.4479 \cdot 10^{-1}$	1.60	$9.7390 \cdot 10^{-1}$
0.100	$3.2804 \cdot 10^{-4}$	0.390	$4.6382 \cdot 10^{-1}$	1.70	$9.7777 \cdot 10^{-1}$
0.110	$9.2957 \cdot 10^{-4}$	0.400	$4.8227 \cdot 10^{-1}$	1.80	$9.8091 \cdot 10^{-1}$
0.120	$2.1727 \cdot 10^{-3}$	0.420	$5.1738 \cdot 10^{-1}$	1.90	$9.8349 \cdot 10^{-1}$
0.130	$4.3866 \cdot 10^{-3}$	0.440	$5.5012 \cdot 10^{-1}$	2.00	$9.8563 \cdot 10^{-1}$

APPENDIX B.   LOOK-UP TABLE

Temperature and Radiance
Conversion And Look-up Table

```
%   Numerical Integration for Planck's law
%   Integration by midpoint rule
%   Matlab program with look-up table outputs

clear;
Tmin=283.;   % <--- Guess T to obtain the corresponding radiance
dT=0.01;
n=200;

disp(' Temperature      Radiance');
disp(' ------------    ---------------');
h=6.626e-34;   c=2.998e8;   k=1.382e-23;
a=8e-6;   b=12e-6;   dx=0.001e-6;

 for T=Tmin:dT:Tmin+n*dT

   sf=0.0;

   for x=a:dx:b-dx

     xm=x+dx/2;           % midpoint of f(x)

     f1=(2*h*c^2)/(xm^5);
     f2=1/(exp((h*c)/(xm*k*T))-1);
     fx=f1*f2;
     sf=sf+fx*dx;

   end;

   disp([T,sf]);

  end;

end;
```

Look-up Table for Temperature and Radiance Conversions

Temperature (K)	Radiance (W/m^2Sr)
283.0000	28.8410
283.0500	28.8673
283.1000	28.8937
283.1500	28.9201
283.2000	28.9464
283.2500	28.9728
283.3000	28.9993
283.3500	29.0257
283.4000	29.0521
283.4500	29.0786
283.5000	29.1051
283.5500	29.1316
283.6000	29.1581
283.6500	29.1846
283.7000	29.2111
283.7500	29.2377
283.8000	29.2642
283.8500	29.2908
283.9000	29.3174
283.9500	29.3440
284.0000	29.3706
284.0500	29.3973
284.1000	29.4239
284.1500	29.4506
284.2000	29.4773
284.2500	29.5040
284.3000	29.5307
284.3500	29.5574
284.4000	29.5842
284.4500	29.6110
284.5000	29.6377
284.5500	29.6645
284.6000	29.6913
284.6500	29.7182
284.7000	29.7450
284.7500	29.7719

```
284.8000   29.7987
284.8500   29.8256
284.9000   29.8525
284.9500   29.8794
285.0000   29.9064
285.0500   29.9333
285.1000   29.9603
285.1500   29.9872
285.2000   30.0142
285.2500   30.0412
285.3000   30.0683
285.3500   30.0953
285.4000   30.1224
285.4500   30.1494
285.5000   30.1765
```

APPENDIX C. AUXILIARY PROGRAM (SEARAD CODE)

A. INTRODUCTION

"SEARAD" is a modified MODTRAN2 code that predicts sea radiance between 52.63 cm^{-1} and 25000 cm^{-1}. MODTRAN is a computer code designed to determine atmospheric transmission and radiance at moderate resolution from 0 to 50,000 cm^{-1}. It is based on AFGL's LOWTRAN7 code. SEARAD is based on the Cox-Munk (Cox and Munk, 1954,1956) statistical model for wind-driven capillary wave facets. An individual facet is chosen and a specific slope is given with respect to the local horizon. The facet is allowed to reflect the sky and sun and emit thermal black body radiation toward an observer. We can find the total radiance by applying proper weight to the facet and integrating over all facets within the observer's field of view.

"SEARAD" can be used in a spectral range from the visible to the far infrared regime. It is a DOS-compatible program that runs on a personal computer and calculates sea radiance. The operation of SEARAD is very similar to the original MODTRAN2 code except for some additional new routines to compute the spectral radiance from sun, sky and sea. A new logical switch "SeaSwitch" is required in the input file to activate the radiance calculation. Sun glint is also include in the sea radiance prediction. Preliminary comparisons with data show that SEARAD has an accuracy approximately " several °C in the infrared".[Ref. 1, p. 4]

SEARAD is currently designed for a single pixel and takes about 10 s to execute. Each time a new geometry is chosen by the user. SEARAD recalculates the source radiance and the path radiance and transmission. However, only the path properties change significantly from one pixel to the next in an ocean image.

B. UNZIP SEARAD (INSTALLATION)

The following statement tells how to unzip and run "SEARAD". The zipped files span three disks altogether. The last disk will be disk 3, the first disk will be disk 1. These

commands assume that the hard disk in the computer is drive c:, and that the 3 1/2 inch disks will be loaded into drive a:. If another drive is used instead for the 3 1/2 disks, the drive letter (b: for example) should be substituted for a: in the following instructions.

Sentences in parentheses are physical acts; sentences without parentheses are commands that should be typed on the keyboard.

To unzip:

     c:\ mkdir searad

     cd searad (Insert disk1 in drive a:)

     copy a:\pkunzip.exe

     pkunzip a:\source

     pkunzip a:\input

     pkunzip a:\exe   (Follow instructions for disk insertion.)

The files should all be unzipped at this point. The directory c:\searad should now contain:

     zip utility : pkunzip.exe

     source code : Modnn [nn=10 to 22 (except mod21.for)

     Input file : Tape5xxx.std

     Log of mods : Note.txt

     Executables : Searad.exe, Dirac, and DOSxmsf.exe

To run Searad :

     copy tape5rad.std tape5

     searad

     type out

This should show the output file corresponding to the input file " Tape5rad.std ".

C.   SEARAD SAMPLE DESCRIPTION

In this section an example is provided to show how to use SEARAD to predict ocean radiance. An input file called " Tape5rad.std " (Table 14) employs a 1976 U.S. standard atmosphere to calculate ocean radiance observed at a zenith angle of 100 degree from a height of 23 m. The Navy aerosol model is used. The calculation is done with

multiple scattering at low spectral resolution (LOWTRAN 7) for a single wave number (945 cm) in the long wave band. The meanings of each " Card " field in the input file (Tape5rad.std) in SEARAD are interpreted in details in Appendix D. [Ref. 1, pp. 3-12] The following DOS commands will calculate ocean radiance and print results

    copy tape5.std tape5

    searad

    type out

These commands produce an output file called "out" (Table 15) . The four contributions to ocean radiance (path to footprint, sea emission, sky reflection, and sun glint) are listed at the end of the "out" file. "TBOUND" in the input file here is interpreted as sea temperature.

There are two new parameters in the input file at the end of the third line: "90.000" and "T". The "T" (stands for true), which may appear anywhere in columns 76 through 80 of the third line of the input file (at the end of card 3), is a new logical parameter "Seaswitch." The parameter is required or a fatal error will be generated in the input file. "Seaswitch" controls the sea radiance calculation. When "Seaswitch" is equal to "T," the sea radiance calculation will be allowed provided certain other conditions are met. When it is equal to "F" (stands for false), the sea radiance calculation will be prevented under all conditions and the program will execute as originally released by the Air Force.

The "90.000," which may appear anywhere in column 66 to 75 of the third line of the input file (near the end of the input file), is a new floating parameter. The program will run whether the parameter is included in the input file or not. It is the azimuth of the upwind direction measured from the line of sight in degrees positive East of North. If the field is blank, meaning that the observer is looking directly into the wind. In the input file in Table 14, the parameter "90" means that the wind is blowing from right to left, perpendicular to the direction of observation. [Ref. 1, pp. 4-5]

D. SEARAD MODEL

The SEARAD model computes four contributions to sea radiance. The assumption for the model is that the strength of interaction between an optical ray and a capillary wave facet is given by the facet area projected normal to the ray. It does not include multiple reflections, shadowing and gravity waves. It also ignores polarization. Each of the four contributions is shown in Figure 14.

The first contribution is path radiance (N_{path}), which is shown on top of Figure 14. The footprint of a single pixel in an image of the sea is indicated by the wavy line. The footprint is observed by a receiver at the end of a ray whose zenith angle at the footprint is θ_r. N_{path} represents the spectral radiance in W/m^2 /sr/cm along the path from the footprint to the receiver.

The second contribution is reflected sky radiance (N_{sky}). The spectral radiance N_s from part of the sky reaches the footprint along a ray whose zenith angle is θ_s. The contributions are the summation from all portions of the sky after specular reflection by the appropriate facets within the footprint. N_{sky} is the sum leaving the footprint at zenith angle θ_s. During its path to the receiver, N_{sky} is attenuated by the path transmission τ_{path}.

The third contribution is reflected solar radiance (N_{sun}), sun glint . The radiance N_o from the solar center arrives at the footprint along a path whose zenith angle is θ_o. Within the footprint most facets deflect the solar ray away from the receiver and are rejected, but some facets are retained because they deflect the ray specularly toward the receiver along a path with zenith angle θ_r. N_{sun} is the spectral radiance leaving the footprint after summation over rays arriving from all portions of the solar disk. N_{sun} is also attenuated by the path transmission τ_{path} .

The fourth contribution is thermal black body emission (N_{sea}). In this portion each facet emits a spectral radiance N_{bb} given by Planck's equation for a black body. The sea temperature is equal to the value of TBOUND in the input file. The spectral emissivity of a given facet in the direction of the receiver is specified by the slope of that facet and the value of θ_r. N_{sea} is the thermal spectral radiance leaving the footprint for the receiver after

70

summation over all facets within the footprint. N_{sea} is also attenuated by path transmission τ_{path} after leaving the footprint.

The symbol ρ in Figure 14 represents the reflectivity of sea water. It is calculated from Fresnel's equations. The total spectral radiance $N(v)$ received at wave number $v(\text{cm-1})$ is given in Equation (19)

$$N(v) = N_{path}(v)f(v) + \left[N_{sky}(v) + N_{sun}(v) + N_{sea}(v)\right]\tau_{path}(v)f(v) , \qquad \textbf{(19)}$$

where $f(v)$ stands for the spectral responsivity of the receiver.

The design of SEARAD is such that the path (N_{path}, τ_{path}) and source (N_s, N_o, N_{bb}) values are taken from the original MODTRAN 2 while Fresnel reflection (ρ) and slope integrated values $(N_{sky}, N_{sun}, N_{sea})$ are introduced in new subroutines. Integration of Equation(19) over the wave number band specified in the input file (Tape5) is implemented in a modification of subroutine "TRAN" to produce the band integrated values for sea radiance given in the output file (out). [Ref. 1, pp. 6-7]
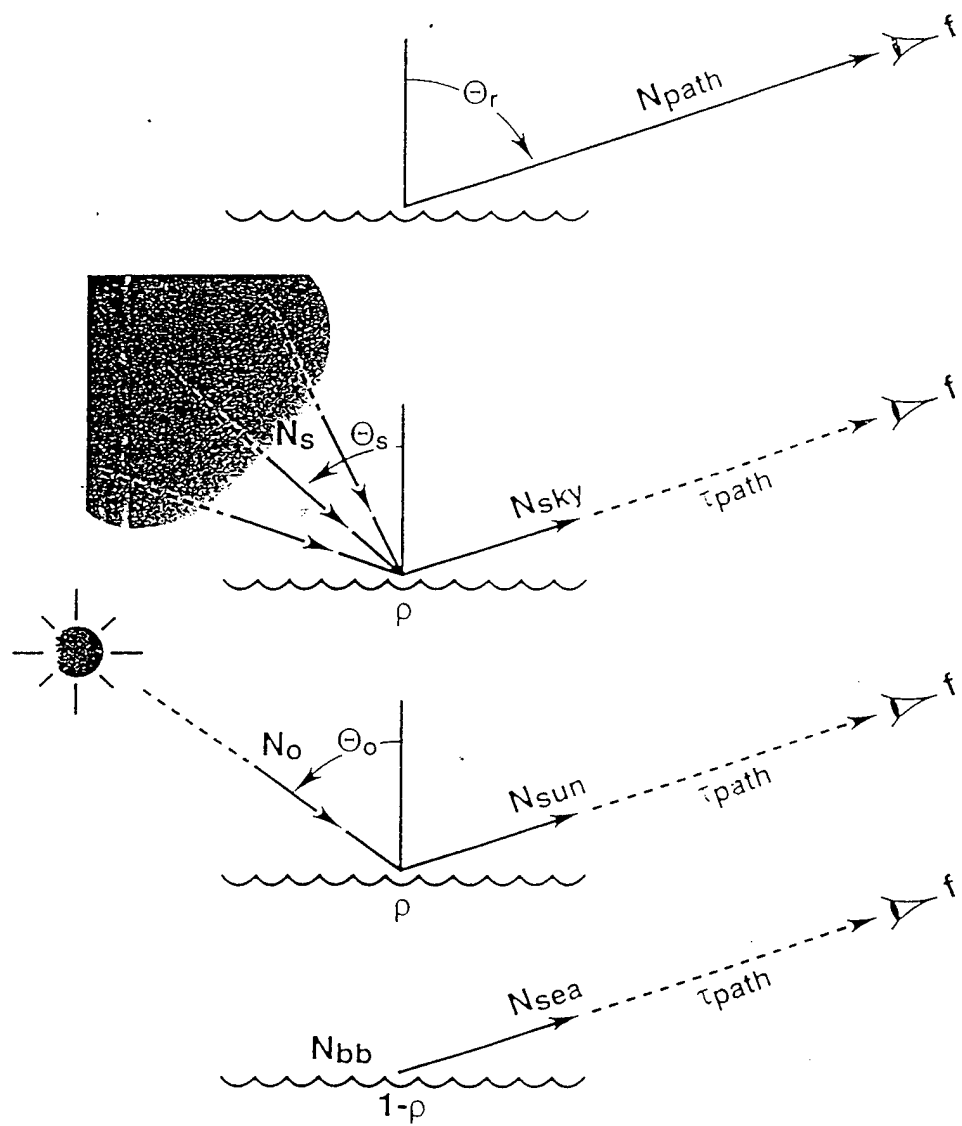
$$N = (\ N_{sky} + N_{sun} + N_{sea}\ )\tau_{path} \circ f + N_{path} \circ f$$

Figure 14. Four Contributions to Sea Radiance in SEARAD Model
From [Ref. 1, Figure 1]

Table 14. SEARAD Input File Sample (Tape5rad.std)

```
F  6  3  1  1 0  0  0  0  0  0  0  0  0 288.15 0.0

3  0  0  5  0 0  10.00  10.00  10.00 0.00  0.00

0.023   0.00 100.00  0.0  0.0  0.0  0   90.0  T

940      950     10      5

0
```

"TAPE5RAD.STD" for Sky3.in
Lowtran radiance
1976 U. S. Standard Atm
Sea switched on
Slant Path to space:
   23 m
   100 degrees
Wind az 90.00 wrt Look
Thermal mode
TBOUND = 15 C = Tsea
No MS reflections:
SALB = 0.
Air Mass 5
Visibility 10 km
Current wind 10 m s-1
Average wind 10 m s-1
Narrow band at 945 cm-1

Table 15. SEARAD Output File Sample (out)

***** SEARAD, A MODIFICATION OF LOWTRAN7 *****

DATE: 06/09/1996
THERMAL RADIANCE MODE
MULTIPLE SCATTERING USED
MARINE AEROSOL MODEL USED
WIND SPEED   =   10.00 M/SEC
WIND SPEED   =   10.00 M/SEC, 24 HR AVERAGE
RELATIVE HUMIDITY =   50.00 PERCENT
AIRMASS CHARACTER =   5.0
VISIBILITY =10.00 KM
SLANT PATH TO SPACE
     H1   =   .023 KM
     HMIN   =   .000 KM
     ANGLE =   100.000 DEG
FREQUENCY RANGE
     IV1   =   940 CM-1 (10.64 MICROMETERS)
     IV2   =   950 CM-1 (10.53 MICROMETERS)
     IDV   =   10 CM-1
     IFWHM =   5 CM-1
     IFILTER =   0
SEA AT 288.15 K REPLACES BLACK BODY BOUNDARY
     UPWIND =   90.000 DEG EAST OF LINE OF SIGHT
ZERO RANGE VALUES
     SEA EMISSION   = .72334 W M-2 SR-1 (AV. EMISS. .7989)
     SKY REFLECTION   = .06266 W M-2 SR-1
     SUN GLINT   = .00000 W M-2 SR-1
     TOTAL RADIANCE   = .78599 W M-2 SR-1
     BLACK BODY TEMP.=   6.7 C
FULL RANGE VALUES
     PATH TO FOOTPRINT = .01814 W M-2 SR-1(AV. TRANS. .9776)
     SEA EMISSION   = .70712 W M-2 SR-1
     SKY REFLECTION   = .06125 W M-2 SR-1
     SUN GLINT   = .00000 W M-2 SR-1
TOTAL RADIANCE   = .78652 W M-2 SR-1
     BLACK BODY TEMP =   6.7 C

APPENDIX D. DESCRIPTION OF EACH CARD IN SEARAD INPUT FILE

In this input file, the format is very important. Each number must be in the correct location. Below is a listing of the input file parameters in SEARAD and the values used in evaluating the sea radiance. The definition of each value is included. The xx's serve as place holders for actual values.

CARD 1 (line one)

F $\Rightarrow$ use LOWTRAN 7

7 $\Rightarrow$ MODEL : radiosonde data used

3 $\Rightarrow$ ITYPE : slant path to space

1 $\Rightarrow$ IEMSCT : program execution in radiance mode

1 $\Rightarrow$ IMULT : program executed with multiple scattering

      "M1,M2,M3" are used to modify or supplement the altitude profiles of

      temperature and pressure, water vapor, and ozone "M4,M5,M6"

xx $\Rightarrow$ M1 : default temperature and pressure to specified MODEL

      atmosphere (M1=1~6)

xx $\Rightarrow$ M2 : default H_2O to specified MODEL atmosphere (M2=1~6)

xx $\Rightarrow$ M3 : default ozone to specified MODEL atmosphere (M3=1~6)

xx $\Rightarrow$ M4 : default CH4 to specified MODEL atmosphere (M4=1~6)

xx $\Rightarrow$ M5 : default N_2O to specified MODEL atmosphere (M5=1~6)

xx $\Rightarrow$ M6 : default CO to specified MODEL atmosphere (M6=1~6)

1 $\Rightarrow$ MDEF use default profile for CO2, O2, NO, SO2, NO2, NH3, HNO3

1 $\Rightarrow$ IM : radiosonde data to be read initially

1 $\Rightarrow$ NORPT : minimize printing of transmittance

xx $\Rightarrow$ TBOUND : boundary temperature ($^{\circ}k$)

0.00 $\Rightarrow$ SALB : surface albedo (0.0 to 1.0)

CARD 2 (line 2)

3 $\Rightarrow$ IHAZE : navy maritime extinction, sets own VIS.

0 $\Rightarrow$ ISEASN : Summer for model 7

0 $\Rightarrow$ IVULCN : default to stratospheric background

16 $\Rightarrow$ ICSTL : air mass character for 1.6. (1 for open ocean - 10 for strong continental influence) ICSTL now allow non-integer values. Integers from 1 to 10 inclusive will be taken as is, while integers from 11 to 300 inclusive will be divided by 10. Integers outside the range of 1 to 300 will be reset to a default value of "3.0".

0 $\Rightarrow$ ICLD : no clouds or rain

0 $\Rightarrow$ IVSA : not used

xx $\Rightarrow$ VIS : meteorological range

xx $\Rightarrow$ WSS : specifies current wind speed (m/s)

xx $\Rightarrow$ WSS : 24 hour average wind speed (m/s)

0.00 $\Rightarrow$ RAINT : rain rate (mm/hr)

0.00 $\Rightarrow$ GNDALT altitude of surface relative to sea level (km)

CARD 2c (line 3)

33 $\Rightarrow$ ML : number of atmospheric layers to be inserted

0 $\Rightarrow$ IRD1 : no read

0 $\Rightarrow$ IRD2 : no read

text TITLE : user defined text

CARD 2c1 (next 33 line)

xx $\Rightarrow$ ZMDL : altitude of layer (km)

xx $\Rightarrow$ P : pressure at layer (mb)

xx   ⇒ T ambient temperature (°C)

xx   ⇒ JCHAR(RH) : relative humidity (%)

ABH ⇒ set units for P,T,RH

CARD 3 (line 37)

xx   ⇒ H1 : initial altitude (FLIR sensor altitude) (km)

0.00 ⇒ H2 : final altitude (seasurface altitude) (km)

xx   ⇒ ANGLE : zenith angle (degree)

0.000 ⇒ RANGE : path length (km)

0.000 ⇒ BETA : earth center angle subtented by H! and H2 (degree)

0.000 ⇒ RO : default radius of earth (km)

0.000 ⇒ LEN normal operation of program (1 for long path through tangent height)

90.00 ⇒ Psi : azimuth of the upwind direction from line of sight positive East of North (degree) 90 ° means that the wind is blowing from right to left, perpendicular to the direction of observation

T   ⇒ True : sea radiance will be carried out (F means that sea radiance will be prevented under all conditions)

CARD 4 (line 38)

830   ⇒ V1 : initial wave number (cm^{-1})

1250 ⇒ V2 : final wave number (cm^{-1})

10   ⇒ DV : wave number increment (cm^{-1})

0   ⇒ no filter

CARD 5

0   ⇒ IRPT : end program (3 means read CARD 3 again)

APPENDIX E. SEARAD INPUT DATA

Detection Range, RUN 1

```
F   7   3   1   1   6   6   6      6      6      6      1      1   1   284.70   0.000
    3   0   0   16  0   0   27.080    10.19   10.50   0.000   0.000
    29  0   0   Aug.04 1992,0411 PORT Aspect
    0.007   1013.600   12.200    94.0    ABH
    0.025   1011.625   12.280    92.4    ABH
    0.050   1008.881   12.390    90.2    ABH
    0.075   1005.709   12.499    88.0    ABH
    0.120   1000.000   12.700    84.0    ABH
    0.208   989.500    12.300    84.0    ABH
    0.253   984.200    12.200    84.0    ABH
    0.270   982.300    12.900    83.0    ABH
    0.365   971.300    16.700    30.0    ABH
    0.543   951.400    23.700     6.0    ABH
    0.558   949.800    24.300     6.0    ABH
    0.771   926.800    25.600     4.0    ABH
    1.525   850.000    21.700     7.0    ABH
    3.174   700.000    12.400     5.0    ABH
    3.182   699.300    12.300     5.0    ABH
    4.017   632.100     5.200    14.0    ABH
    4.514   594.600     3.900     4.0    ABH
    4.974   561.600     0.000     6.0    ABH
    4.984   560.900     0.000     5.0    ABH
    5.891   500.000    -6.700     7.0    ABH
    6.295   474.700   -10.400    11.0    ABH
    6.856   441.000   -13.700     6.0    ABH
    6.880   439.600   -13.800    25.0    ABH
    6.912   437.800   -14.100     8.0    ABH
    7.590   400.000   -19.100     4.0    ABH
    8.037   376.600   -21.800     5.0    ABH
    8.184   369.100   -23.100    10.0    ABH
    8.232   366.700   -23.500    36.0    ABH
    8.284   364.100   -24.000    14.0    ABH

    0.3130   0.000   90.850   0.000   0.000   0.000   1   298.911   T
    830      1250    10       10      0
    0
```

Detection Range, RUN 2

```
F   7   3   1   1   6   6   6       6       6       6       1       1   1   284.70      0.000
        3   0   0   16  0   0   27.080      11.68   10.50   .000    .000
        29  0   0   Aug.04 1992,0425, STBD
        0.007   1013.600    12.200    94.0    ABH
        0.025   1011.625    12.280    92.4    ABH
        0.050   1008.881    12.390    90.2    ABH
        0.075   1005.709    12.499    88.0    ABH
        0.120   1000.000    12.700    84.0    ABH
        0.208   989.500     12.300    84.0    ABH
        0.253   984.200     12.200    84.0    ABH
        0.270   982.300     12.900    83.0    ABH
        0.365   971.300     16.700    30.0    ABH
        0.543   951.400     23.700    6.0     ABH
        0.558   949.800     24.300    6.0     ABH
        0.771   926.800     25.600    4.0     ABH
        1.525   850.000     21.700    7.0     ABH
        3.174   700.000     12.400    5.0     ABH
        3.182   699.300     12.300    5.0     ABH
        4.017   632.100     5.200     14.0    ABH
        4.514   594.600     3.900     4.0     ABH
        4.974   561.600     0.000     6.0     ABH
        4.984   560.900     0.000     5.0     ABH
        5.891   500.000     -6.700    7.0     ABH
        6.295   474.700     -10.400   11.0    ABH
        6.856   441.000     -13.700   6.0     ABH
        6.880   439.600     -13.800   25.0    ABH
        6.912   437.800     -14.100   8.0     ABH
        7.590   400.000     -19.100   4.0     ABH
        8.037   376.600     -21.800   5.0     ABH
        8.184   369.100     -23.100   10.0    ABH
        8.232   366.700     -23.500   36.0    ABH
        8.284   364.100     -24.000   14.0    ABH

        0.3072  .000    91.197  .000    .000    0.000   1   289.438     T
        830         1250    10      10      0
        0
```

Detection Range, RUN 3

```
 F   7  3   1   1   6   6   6        6       6       6      1       1   1   284.70    0.000
     3  0   0   16  0   0   27.080    12.12   10.50   .000    .000
    29  0   0   Aug.04  1992,0432, STN
       0.007  1013.600    12.200    94.0    ABH
       0.025  1011.625    12.280    92.4    ABH
       0.050  1008.881    12.390    90.2    ABH
       0.075  1005.709    12.499    88.0    ABH
       0.120  1000.000    12.700    84.0    ABH
       0.208   989.500    12.300    84.0    ABH
       0.253   984.200    12.200    84.0    ABH
       0.270   982.300    12.900    83.0    ABH
       0.365   971.300    16.700    30.0    ABH
       0.543   951.400    23.700     6.0    ABH
       0.558   949.800    24.300     6.0    ABH
       0.771   926.800    25.600     4.0    ABH
       1.525   850.000    21.700     7.0    ABH
       3.174   700.000    12.400     5.0    ABH
       3.182   699.300    12.300     5.0    ABH
       4.017   632.100     5.200    14.0    ABH
       4.514   594.600     3.900     4.0    ABH
       4.974   561.600     0.000     6.0    ABH
       4.984   560.900     0.000     5.0    ABH
       5.891   500.000    -6.700     7.0    ABH
       6.295   474.700   -10.400    11.0    ABH
       6.856   441.000   -13.700     6.0    ABH
       6.880   439.600   -13.800    25.0    ABH
       6.912   437.800   -14.100     8.0    ABH
       7.590   400.000   -19.100     4.0    ABH
       8.037   376.600   -21.800     5.0    ABH
       8.184   369.100   -23.100    10.0    ABH
       8.232   366.700   -23.500    36.0    ABH
       8.284   364.100   -24.000    14.0    ABH

     0.3109   .000   91.390   .000   .000   0.000   1   283.893   T
      830     1250    10       10      0
       0
```

Detection Range, RUN 4

| F | 7 | 3 | 1 | 1 | 6 | 6 | 6 | 6 | 6 | 6 | 1 | 1 | 1 | 284.70 | 0.000 |

| 3 | 0 | 0 | 16 | 0 | 0 | 27.080 | 13.26 | 10.50 | .000 | .000 |

29 0 0   Aug. 04 1992, 0441, BOW Aspect

0.007	1013.600	12.200	94.0	ABH
0.025	1011.625	12.280	92.4	ABH
0.050	1008.881	12.390	90.2	ABH
0.075	1005.709	12.499	88.0	ABH
0.120	1000.000	12.700	84.0	ABH
0.208	989.500	12.300	84.0	ABH
0.253	984.200	12.200	84.0	ABH
0.270	982.300	12.900	83.0	ABH
0.365	971.300	16.700	30.0	ABH
0.543	951.400	23.700	6.0	ABH
0.558	949.800	24.300	6.0	ABH
0.771	926.800	25.600	4.0	ABH
1.525	850.000	21.700	7.0	ABH
3.174	700.000	12.400	5.0	ABH
3.182	699.300	12.300	5.0	ABH
4.017	632.100	5.200	14.0	ABH
4.514	594.600	3.900	4.0	ABH
4.974	561.600	0.000	6.0	ABH
4.984	560.900	0.000	5.0	ABH
5.891	500.000	-6.700	7.0	ABH
6.295	474.700	-10.400	11.0	ABH
6.856	441.000	-13.700	6.0	ABH
6.880	439.600	-13.800	25.0	ABH
6.912	437.800	-14.100	8.0	ABH
7.590	400.000	-19.100	4.0	ABH
8.037	376.600	-21.800	5.0	ABH
8.184	369.100	-23.100	10.0	ABH
8.232	366.700	-23.500	36.0	ABH
8.284	364.100	-24.000	14.0	ABH

| 0.3088 | .000 | 91.209 | .000 | .000 | 0.000 | 1 | 275.374 | T |

| 830 | 1250 | 10 | 10 | 0 |

0

Detection Range, RUN 5

F 7 3 1 1 6 6 6 6 6 6 1 1 1 284.70 0.000
  3 0 0 16 0 0 27.080 12.04 10.50 .000 .000
  29 0 0 Aug. 04 1992, 0441, 0449, STBD

0.007	1013.600	12.200	94.0	ABH
0.025	1011.625	12.280	92.4	ABH
0.050	1008.881	12.390	90.2	ABH
0.075	1005.709	12.499	88.0	ABH
0.120	1000.000	12.700	84.0	ABH
0.208	989.500	12.300	84.0	ABH
0.253	984.200	12.200	84.0	ABH
0.270	982.300	12.900	83.0	ABH
0.365	971.300	16.700	30.0	ABH
0.543	951.400	23.700	6.0	ABH
0.558	949.800	24.300	6.0	ABH
0.771	926.800	25.600	4.0	ABH
1.525	850.000	21.700	7.0	ABH
3.174	700.000	12.400	5.0	ABH
3.182	699.300	12.300	5.0	ABH
4.017	632.100	5.200	14.0	ABH
4.514	594.600	3.900	4.0	ABH
4.974	561.600	0.000	6.0	ABH
4.984	560.900	0.000	5.0	ABH
5.891	500.000	-6.700	7.0	ABH
6.295	474.700	-10.400	11.0	ABH
6.856	441.000	-13.700	6.0	ABH
6.880	439.600	-13.800	25.0	ABH
6.912	437.800	-14.100	8.0	ABH
7.590	400.000	-19.100	4.0	ABH
8.037	376.600	-21.800	5.0	ABH
8.184	369.100	-23.100	10.0	ABH
8.232	366.700	-23.500	36.0	ABH
8.284	364.100	-24.000	14.0	ABH

0.1393 .000 90.364 .000 .000 0.000 1 277.645 T
830 1250 10 10 0
0

Detection Range, RUN 6

F 7 3 1 1 6 6 6   6   6   6   1   1 1 284.70 0.000
      3 0 0 16 0 0 27.080   8.277 10.50   .000   .000
      29 0 0 Aug. 04 1992, 0503, PORT Aspect

0.007	1013.600	12.200	94.0	ABH
0.025	1011.625	12.280	92.4	ABH
0.050	1008.881	12.390	90.2	ABH
0.075	1005.709	12.499	88.0	ABH
0.120	1000.000	12.700	84.0	ABH
0.208	989.500	12.300	84.0	ABH
0.253	984.200	12.200	84.0	ABH
0.270	982.300	12.900	83.0	ABH
0.365	971.300	16.700	30.0	ABH
0.543	951.400	23.700	6.0	ABH
0.558	949.800	24.300	6.0	ABH
0.771	926.800	25.600	4.0	ABH
1.525	850.000	21.700	7.0	ABH
3.174	700.000	12.400	5.0	ABH
3.182	699.300	12.300	5.0	ABH
4.017	632.100	5.200	14.0	ABH
4.514	594.600	3.900	4.0	ABH
4.974	561.600	0.000	6.0	ABH
4.984	560.900	0.000	5.0	ABH
5.891	500.000	-6.700	7.0	ABH
6.295	474.700	-10.400	11.0	ABH
6.856	441.000	-13.700	6.0	ABH
6.880	439.600	-13.800	25.0	ABH
6.912	437.800	-14.100	8.0	ABH
7.590	400.000	-19.100	4.0	ABH
8.037	376.600	-21.800	5.0	ABH
8.184	369.100	-23.100	10.0	ABH
8.232	366.700	-23.500	36.0	ABH
8.284	364.100	-24.000	14.0	ABH

0.1548   .000   90.570   .000   .000   0.000 1 295.427 T
830   1250   10   10   0
0

84

Detection Range, RUN 7

```
F   7   3   1   1   6   6   6       6       6       6       1       1   1   284.70      0.000
    3   0   0   16  0   0   27.080  8.277   10.50   .000    .000
    29  0   0   Aug. 04 1992,0511, STBD Aspect
    0.007   1013.600    12.200  94.0    ABH
    0.025   1011.625    12.280  92.4    ABH
    0.050   1008.881    12.390  90.2    ABH
    0.075   1005.709    12.499  88.0    ABH
    0.120   1000.000    12.700  84.0    ABH
    0.208   989.500     12.300  84.0    ABH
    0.253   984.200     12.200  84.0    ABH
    0.270   982.300     12.900  83.0    ABH
    0.365   971.300     16.700  30.0    ABH
    0.543   951.400     23.700  6.0     ABH
    0.558   949.800     24.300  6.0     ABH
    0.771   926.800     25.600  4.0     ABH
    1.525   850.000     21.700  7.0     ABH
    3.174   700.000     12.400  5.0     ABH
    3.182   699.300     12.300  5.0     ABH
    4.017   632.100     5.200   14.0    ABH
    4.514   594.600     3.900   4.0     ABH
    4.974   561.600     0.000   6.0     ABH
    4.984   560.900     0.000   5.0     ABH
    5.891   500.000     -6.700  7.0     ABH
    6.295   474.700     -10.400 11.0    ABH
    6.856   441.000     -13.700 6.0     ABH
    6.880   439.600     -13.800 25.0    ABH
    6.912   437.800     -14.100 8.0     ABH
    7.590   400.000     -19.100 4.0     ABH
    8.037   376.600     -21.800 5.0     ABH
    8.184   369.100     -23.100 10.0    ABH
    8.232   366.700     -23.500 36.0    ABH
    8.284   364.100     -24.000 14.0    ABH

    0.1640  .000    90.428  .000    .000    0.000   1   289.911     T
    830     1250    10      10      0
    0
```

Detection Range, RUN 8

F 7 3 1 1 6 6 6   6   6   6   1   1 1 284.70 0.000

   3 0 0 16 0 0 27.080 7.943 10.50 .000 .000

   29 0 0 Aug. 04 1992, 0522, PORT

0.007	1013.600	12.200	94.0	ABH
0.025	1011.625	12.280	92.4	ABH
0.050	1008.881	12.390	90.2	ABH
0.075	1005.709	12.499	88.0	ABH
0.120	1000.000	12.700	84.0	ABH
0.208	989.500	12.300	84.0	ABH
0.253	984.200	12.200	84.0	ABH
0.270	982.300	12.900	83.0	ABH
0.365	971.300	16.700	30.0	ABH
0.543	951.400	23.700	6.0	ABH
0.558	949.800	24.300	6.0	ABH
0.771	926.800	25.600	4.0	ABH
1.525	850.000	21.700	7.0	ABH
3.174	700.000	12.400	5.0	ABH
3.182	699.300	12.300	5.0	ABH
4.017	632.100	5.200	14.0	ABH
4.514	594.600	3.900	4.0	ABH
4.974	561.600	0.000	6.0	ABH
4.984	560.900	0.000	5.0	ABH
5.891	500.000	-6.700	7.0	ABH
6.295	474.700	-10.400	11.0	ABH
6.856	441.000	-13.700	6.0	ABH
6.880	439.600	-13.800	25.0	ABH
6.912	437.800	-14.100	8.0	ABH
7.590	400.000	-19.100	4.0	ABH
8.037	376.600	-21.800	5.0	ABH
8.184	369.100	-23.100	10.0	ABH
8.232	366.700	-23.500	36.0	ABH
8.284	364.100	-24.000	14.0	ABH

0.1615 .000 90.595 .000 .000 0.000 1 293.928 T

830   1250   10   10   0

0

Classification, RUN 1

F 7 3 1 1 6 6 6   6   6   6   1   1 1 284.70 0.000
   3 0 0 16 0 0 27.080   10.19   10.50   .000   .000
   29 0 0 Aug. 04 1992, 0411 PORT Aspect

0.025	1011.625	12.280	92.4	ABH
0.007	1013.600	12.200	94.0	ABH
0.050	1008.881	12.390	90.2	ABH
0.075	1005.709	12.499	88.0	ABH
0.120	1000.000	12.700	84.0	ABH
0.208	989.500	12.300	84.0	ABH
0.253	984.200	12.200	84.0	ABH
0.270	982.300	12.900	83.0	ABH
0.365	971.300	16.700	30.0	ABH
0.543	951.400	23.700	6.0	ABH
0.558	949.800	24.300	6.0	ABH
0.771	926.800	25.600	4.0	ABH
1.525	850.000	21.700	7.0	ABH
3.174	700.000	12.400	5.0	ABH
3.182	699.300	12.300	5.0	ABH
4.017	632.100	5.200	14.0	ABH
4.514	594.600	3.900	4.0	ABH
4.974	561.600	0.000	6.0	ABH
4.984	560.900	0.000	5.0	ABH
5.891	500.000	-6.700	7.0	ABH
6.295	474.700	-10.400	11.0	ABH
6.856	441.000	-13.700	6.0	ABH
6.880	439.600	-13.800	25.0	ABH
6.912	437.800	-14.100	8.0	ABH
7.590	400.000	-19.100	4.0	ABH
8.037	376.600	-21.800	5.0	ABH
8.184	369.100	-23.100	10.0	ABH
8.232	366.700	-23.500	36.0	ABH
8.284	364.100	-24.000	14.0	ABH

0.3130 .000 92.180 .000 .000 0.000 1 298.991 T
830   1250 10   10   0
0

Classification Range, RUN 2

| F | .7 | 3 | 1 | 1 | 6 | 6 | 6 | 6 | 6 | 6 | 1 | 1 | 1 | 284.70 | 0.000 |

| 3 | 0 | 0 | 16 | 0 | 0 | 27.080 | 11.68 | 10.50 | .000 | .000 |

| 29 | 0 | 0 | Aug.04 | 1992,0425, | STBD | Aspect |

0.007	1013.600	12.200	94.0	ABH
0.025	1011.625	12.280	92.4	ABH
0.050	1008.881	12.390	90.2	ABH
0.075	1005.709	12.499	88.0	ABH
0.120	1000.000	12.700	84.0	ABH
0.208	989.500	12.300	84.0	ABH
0.253	984.200	12.200	84.0	ABH
0.270	982.300	12.900	83.0	ABH
0.365	971.300	16.700	30.0	ABH
0.543	951.400	23.700	6.0	ABH
0.558	949.800	24.300	6.0	ABH
0.771	926.800	25.600	4.0	ABH
1.525	850.000	21.700	7.0	ABH
3.174	700.000	12.400	5.0	ABH
3.182	699.300	12.300	5.0	ABH
4.017	632.100	5.200	14.0	ABH
4.514	594.600	3.900	4.0	ABH
4.974	561.600	0.000	6.0	ABH
4.984	560.900	0.000	5.0	ABH
5.891	500.000	-6.700	7.0	ABH
6.295	474.700	-10.400	11.0	ABH
6.856	441.000	-13.700	6.0	ABH
6.880	439.600	-13.800	25.0	ABH
6.912	437.800	-14.100	8.0	ABH
7.590	400.000	-19.100	4.0	ABH
8.037	376.600	-21.800	5.0	ABH
8.184	369.100	-23.100	10.0	ABH
8.232	366.700	-23.500	36.0	ABH
8.284	364.100	-24.000	14.0	ABH

| 0.3072 | .000 | 93.853 | .000 | .000 | 0.000 | 1 | 289.438 | T |

| 830 | 1250 | 10 | 10 | 0 |

0

Classification Range, RUN 3

```
F    7  3   1   1   6   6   6        6        6        6        1        1   1   284.70    0.000
     3  0   0   16  0   0   27.080     12.12   10.50    .000     .000
    29  0   0   Aug.04 1992,0432, STN Aspect
    0.007  1013.600   12.200   94.0   ABH
    0.025  1011.625   12.280   92.4   ABH
    0.050  1008.881   12.390   90.2   ABH
    0.075  1005.709   12.499   88.0   ABH
    0.120  1000.000   12.700   84.0   ABH
    0.208   989.500   12.300   84.0   ABH
    0.253   984.200   12.200   84.0   ABH
    0.270   982.300   12.900   83.0   ABH
    0.365   971.300   16.700   30.0   ABH
    0.543   951.400   23.700    6.0   ABH
    0.558   949.800   24.300    6.0   ABH
    0.771   926.800   25.600    4.0   ABH
    1.525   850.000   21.700    7.0   ABH
    3.174   700.000   12.400    5.0   ABH
    3.182   699.300   12.300    5.0   ABH
    4.017   632.100    5.200   14.0   ABH
    4.514   594.600    3.900    4.0   ABH
    4.974   561.600    0.000    6.0   ABH
    4.984   560.900    0.000    5.0   ABH
    5.891   500.000   -6.700    7.0   ABH
    6.295   474.700  -10.400   11.0   ABH
    6.856   441.000  -13.700    6.0   ABH
    6.880   439.600  -13.800   25.0   ABH
    6.912   437.800  -14.100    8.0   ABH
    7.590   400.000  -19.100    4.0   ABH
    8.037   376.600  -21.800    5.0   ABH
    8.184   369.100  -23.100   10.0   ABH
    8.232   366.700  -23.500   36.0   ABH
    8.284   364.100  -24.000   14.0   ABH

    0.3109   .000   97.788   .000   .000   0.000   1   283.893   T
    830     1250    10       10      0
    0
```

Classification Range, RUN 4

```
F  7  3  1  1  6  6  6      6      6      6      1      1  1  284.70   0.000
   3  0  0  16 0  0  27.080   13.26  10.50  .000   .000
   29 0  0  Aug. 04 1992, 0441, BOW Aspect
   0.007  1013.600  12.200   94.0  ABH
   0.025  1011.625  12.280   92.4  ABH
   0.050  1008.881  12.390   90.2  ABH
   0.075  1005.709  12.499   88.0  ABH
   0.120  1000.000  12.700   84.0  ABH
   0.208  989.500   12.300   84.0  ABH
   0.253  984.200   12.200   84.0  ABH
   0.270  982.300   12.900   83.0  ABH
   0.365  971.300   16.700   30.0  ABH
   0.543  951.400   23.700    6.0  ABH
   0.558  949.800   24.300    6.0  ABH
   0.771  926.800   25.600    4.0  ABH
   1.525  850.000   21.700    7.0  ABH
   3.174  700.000   12.400    5.0  ABH
   3.182  699.300   12.300    5.0  ABH
   4.017  632.100    5.200   14.0  ABH
   4.514  594.600    3.900    4.0  ABH
   4.974  561.600    0.000    6.0  ABH
   4.984  560.900    0.000    5.0  ABH
   5.891  500.000   -6.700    7.0  ABH
   6.295  474.700  -10.400   11.0  ABH
   6.856  441.000  -13.700    6.0  ABH
   6.880  439.600  -13.800   25.0  ABH
   6.912  437.800  -14.100    8.0  ABH
   7.590  400.000  -19.100    4.0  ABH
   8.037  376.600  -21.800    5.0  ABH
   8.184  369.100  -23.100   10.0  ABH
   8.232  366.700  -23.500   36.0  ABH
   8.284  364.100  -24.000   14.0  ABH

   0.3088  .000  92.150  .000  .000  0.000  1  275.374  T
   830     1250  10     10    0
   0
```

Classification Range, RUN 5

F	7	3	1	1	6	6	6	6	6	6	1	1	1	284.70	0.000
3	0	0	16	0	0	27.080	12.037	10.50	0.000	.0.000					
29	0	0	Aug. 04 1992, 0441, 0449, STBD												

Aspect

0.007	1013.600	12.200	94.0	ABH
0.025	1011.625	12.280	92.4	ABH
0.050	1008.881	12.390	90.2	ABH
0.075	1005.709	12.499	88.0	ABH
0.120	1000.000	12.700	84.0	ABH
0.208	989.500	12.300	84.0	ABH
0.253	984.200	12.200	84.0	ABH
0.270	982.300	12.900	83.0	ABH
0.365	971.300	16.700	30.0	ABH
0.543	951.400	23.700	6.0	ABH
0.558	949.800	24.300	6.0	ABH
0.771	926.800	25.600	4.0	ABH
1.525	850.000	21.700	7.0	ABH
3.174	700.000	12.400	5.0	ABH
3.182	699.300	12.300	5.0	ABH
4.017	632.100	5.200	14.0	ABH
4.514	594.600	3.900	4.0	ABH
4.974	561.600	0.000	6.0	ABH
4.984	560.900	0.000	5.0	ABH
5.891	500.000	-6.700	7.0	ABH
6.295	474.700	-10.400	11.0	ABH
6.856	441.000	-13.700	6.0	ABH
6.880	439.600	-13.800	25.0	ABH
6.912	437.800	-14.100	8.0	ABH
7.590	400.000	-19.100	4.0	ABH
8.037	376.600	-21.800	5.0	ABH
8.184	369.100	-23.100	10.0	ABH
8.232	366.700	-23.500	36.0	ABH
8.284	364.100	-24.000	14.0	ABH

0.1393	.000	90.545	.000	.000	0.000	1	289.911	T
830	1250	10	10	0				
0								

Classification Range, RUN 6

F	7	3	1	1	6	6	6	6	6	6	1	1	1	284.70	0.000
	3	0	0	16	0	0	27.080	8.277	10.50	.000	.000				
	29	0	0	Aug. 04	1992, 0503, PORT Aspect										

0.007	1013.600	12.200	94.0	ABH
0.025	1011.625	12.280	92.4	ABH
0.050	1008.881	12.390	90.2	ABH
0.075	1005.709	12.499	88.0	ABH
0.120	1000.000	12.700	84.0	ABH
0.208	989.500	12.300	84.0	ABH
0.253	984.200	12.200	84.0	ABH
0.270	982.300	12.900	83.0	ABH
0.365	971.300	16.700	30.0	ABH
0.543	951.400	23.700	6.0	ABH
0.558	949.800	24.300	6.0	ABH
0.771	926.800	25.600	4.0	ABH
1.525	850.000	21.700	7.0	ABH
3.174	700.000	12.400	5.0	ABH
3.182	699.300	12.300	5.0	ABH
4.017	632.100	5.200	14.0	ABH
4.514	594.600	3.900	4.0	ABH
4.974	561.600	0.000	6.0	ABH
4.984	560.900	0.000	5.0	ABH
5.891	500.000	-6.700	7.0	ABH
6.295	474.700	-10.400	11.0	ABH
6.856	441.000	-13.700	6.0	ABH
6.880	439.600	-13.800	25.0	ABH
6.912	437.800	-14.100	8.0	ABH
7.590	400.000	-19.100	4.0	ABH
8.037	376.600	-21.800	5.0	ABH
8.184	369.100	-23.100	10.0	ABH
8.232	366.700	-23.500	36.0	ABH
8.284	364.100	-24.000	14.0	ABH

0.1548	.000	91.940	.000	.000	0.000	1	295.427	T
830	1250	10	10	0				
0								

Classification Range, RUN 7

```
F  7  3  1  1  6  6  6      6      6      6      1      1  1  284.70  0.000
      3  0  0  16  0  0  27.080  8.049  10.50  .000   .000
      29  0  0  Aug. 04 1992,0511, STBD Aspect
      0.007  1013.600  12.200   94.0  ABH
      0.025  1011.625  12.280   92.4  ABH
      0.050  1008.881  12.390   90.2  ABH
      0.075  1005.709  12.499   88.0  ABH
      0.120  1000.000  12.700   84.0  ABH
      0.208   989.500  12.300   84.0  ABH
      0.253   984.200  12.200   84.0  ABH
      0.270   982.300  12.900   83.0  ABH
      0.365   971.300  16.700   30.0  ABH
      0.543   951.400  23.700    6.0  ABH
      0.558   949.800  24.300    6.0  ABH
      0.771   926.800  25.600    4.0  ABH
      1.525   850.000  21.700    7.0  ABH
      3.174   700.000  12.400    5.0  ABH
      3.182   699.300  12.300    5.0  ABH
      4.017   632.100   5.200   14.0  ABH
      4.514   594.600   3.900    4.0  ABH
      4.974   561.600   0.000    6.0  ABH
      4.984   560.900   0.000    5.0  ABH
      5.891   500.000  -6.700    7.0  ABH
      6.295   474.700 -10.400   11.0  ABH
      6.856   441.000 -13.700    6.0  ABH
      6.880   439.600 -13.800   25.0  ABH
      6.912   437.800 -14.100    8.0  ABH
      7.590   400.000 -19.100    4.0  ABH
      8.037   376.600 -21.800    5.0  ABH
      8.184   369.100 -23.100   10.0  ABH
      8.232   366.700 -23.500   36.0  ABH
      8.284   364.100 -24.000   14.0  ABH

      0.1640   .000  91.027   .000   .000  0.000  1  289.911  T
      830     1250   10      10      0
      0
```

Classification Range, RUN 8

F	7	3	1	1	6	6	6	6	6	6	1	1	1	284.70	0.000
	3	0	0	16	0	0	27.080	7.943	10.50	.000	.000				

29 0 0 Aug. 04 1992, 0522, PORT Aspect

0.007	1013.600	12.200	94.0	ABH
0.025	1011.625	12.280	92.4	ABH
0.050	1008.881	12.390	90.2	ABH
0.075	1005.709	12.499	88.0	ABH
0.120	1000.000	12.700	84.0	ABH
0.208	989.500	12.300	84.0	ABH
0.253	984.200	12.200	84.0	ABH
0.270	982.300	12.900	83.0	ABH
0.365	971.300	16.700	30.0	ABH
0.543	951.400	23.700	6.0	ABH
0.558	949.800	24.300	6.0	ABH
0.771	926.800	25.600	4.0	ABH
1.525	850.000	21.700	7.0	ABH
3.174	700.000	12.400	5.0	ABH
3.182	699.300	12.300	5.0	ABH
4.017	632.100	5.200	14.0	ABH
4.514	594.600	3.900	4.0	ABH
4.974	561.600	0.000	6.0	ABH
4.984	560.900	0.000	5.0	ABH
5.891	500.000	-6.700	7.0	ABH
6.295	474.700	-10.400	11.0	ABH
6.856	441.000	-13.700	6.0	ABH
6.880	439.600	-13.800	25.0	ABH
6.912	437.800	-14.100	8.0	ABH
7.590	400.000	-19.100	4.0	ABH
8.037	376.600	-21.800	5.0	ABH
8.184	369.100	-23.100	10.0	ABH
8.232	366.700	-23.500	36.0	ABH
8.284	364.100	-24.000	14.0	ABH

0.1615	.000	91.125	.000	.000	0.000	1	293.928	T
830	1250	10	10	0				

0

Identification Range, RUN 1

F 7 3 1 1 6 6 6   6   6   6   1   1 1 284.70 0.000
    3 0 0 16 0 0 27.080 10.19 10.50 0.000 0.000
    29 0 0 Aug.04 1992,0411 PORT Aspect

0.007	1013.600	12.200	94.0	ABH
0.025	1011.625	12.280	92.4	ABH
0.050	1008.881	12.390	90.2	ABH
0.075	1005.709	12.499	88.0	ABH
0.120	1000.000	12.700	84.0	ABH
0.208	989.500	12.300	84.0	ABH
0.253	984.200	12.200	84.0	ABH
0.270	982.300	12.900	83.0	ABH
0.365	971.300	16.700	30.0	ABH
0.543	951.400	23.700	6.0	ABH
0.558	949.800	24.300	6.0	ABH
0.771	926.800	25.600	4.0	ABH
1.525	850.000	21.700	7.0	ABH
3.174	700.000	12.400	5.0	ABH
3.182	699.300	12.300	5.0	ABH
4.017	632.100	5.200	14.0	ABH
4.514	594.600	3.900	4.0	ABH
4.974	561.600	0.000	6.0	ABH
4.984	560.900	0.000	5.0	ABH
5.891	500.000	-6.700	7.0	ABH
6.295	474.700	-10.400	11.0	ABH
6.856	441.000	-13.700	6.0	ABH
6.880	439.600	-13.800	25.0	ABH
6.912	437.800	-14.100	8.0	ABH
7.590	400.000	-19.100	4.0	ABH
8.037	376.600	-21.800	5.0	ABH
8.184	369.100	-23.100	10.0	ABH
8.232	366.700	-23.500	36.0	ABH
8.284	364.100	-24.000	14.0	ABH

0.3130 0.000 92.803 0.000 0.000 0.000 1 298.991 T
830   1250   10   10   0
0

Identification Range, RUN 2

F 7 3 1 1 6 6 6 6 6 6 1 1 1 284.70 0.000

3 0 0 16 0 0 27.080 11.68 10.50 .000 .000

29 0 0 Aug.04 1992,0425, STBD Aspect

0.007	1013.600	12.200	94.0	ABH
0.025	1011.625	12.280	92.4	ABH
0.050	1008.881	12.390	90.2	ABH
0.075	1005.709	12.499	88.0	ABH
0.120	1000.000	12.700	84.0	ABH
0.208	989.500	12.300	84.0	ABH
0.253	984.200	12.200	84.0	ABH
0.270	982.300	12.900	83.0	ABH
0.365	971.300	16.700	30.0	ABH
0.543	951.400	23.700	6.0	ABH
0.558	949.800	24.300	6.0	ABH
0.771	926.800	25.600	4.0	ABH
1.525	850.000	21.700	7.0	ABH
3.174	700.000	12.400	5.0	ABH
3.182	699.300	12.300	5.0	ABH
4.017	632.100	5.200	14.0	ABH
4.514	594.600	3.900	4.0	ABH
4.974	561.600	0.000	6.0	ABH
4.984	560.900	0.000	5.0	ABH
5.891	500.000	-6.700	7.0	ABH
6.295	474.700	-10.400	11.0	ABH
6.856	441.000	-13.700	6.0	ABH
6.880	439.600	-13.800	25.0	ABH
6.912	437.800	-14.100	8.0	ABH
7.590	400.000	-19.100	4.0	ABH
8.037	376.600	-21.800	5.0	ABH
8.184	369.100	-23.100	10.0	ABH
8.232	366.700	-23.500	36.0	ABH
8.284	364.100	-24.000	14.0	ABH

0.3072 .000 94.818 .000 .000 0.000 1 289.438 T

830 1250 10 10 0

0

Identification Range, RUN 3

F   7   3   1   1   6   6   6   6   6   6   1   1   1   284.70   0.000
     3   0   0   16   0   0   27.080   12.12   10.50   .000   .000
     29   0   0   Aug.04 1992,0432, STN Aspect

0.007	1013.600	12.200	94.0	ABH
0.025	1011.625	12.280	92.4	ABH
0.050	1008.881	12.390	90.2	ABH
0.075	1005.709	12.499	88.0	ABH
0.120	1000.000	12.700	84.0	ABH
0.208	989.500	12.300	84.0	ABH
0.253	984.200	12.200	84.0	ABH
0.270	982.300	12.900	83.0	ABH
0.365	971.300	16.700	30.0	ABH
0.543	951.400	23.700	6.0	ABH
0.558	949.800	24.300	6.0	ABH
0.771	926.800	25.600	4.0	ABH
1.525	850.000	21.700	7.0	ABH
3.174	700.000	12.400	5.0	ABH
3.182	699.300	12.300	5.0	ABH
4.017	632.100	5.200	14.0	ABH
4.514	594.600	3.900	4.0	ABH
4.974	561.600	0.000	6.0	ABH
4.984	560.900	0.000	5.0	ABH
5.891	500.000	-6.700	7.0	ABH
6.295	474.700	-10.400	11.0	ABH
6.856	441.000	-13.700	6.0	ABH
6.880	439.600	-13.800	25.0	ABH
6.912	437.800	-14.100	8.0	ABH
7.590	400.000	-19.100	4.0	ABH
8.037	376.600	-21.800	5.0	ABH
8.184	369.100	-23.100	10.0	ABH
8.232	366.700	-23.500	36.0	ABH
8.284	364.100	-24.000	14.0	ABH

0.3109   .000   109.880   .000   .000   0.000   1   283.893   T
830   1250   10   10   0
0

Identification Range, RUN 4

F 7 3 1 1 6 6 6 6 6 6 1 1 1 284.70 0.000

3 0 0 16 0 0 27.080 13.26 10.50 .000 .000

29 0 0 Aug. 04 1992, 0441, BOW Aspect

0.007	1013.600	12.200	94.0	ABH
0.025	1011.625	12.280	92.4	ABH
0.050	1008.881	12.390	90.2	ABH
0.075	1005.709	12.499	88.0	ABH
0.120	1000.000	12.700	84.0	ABH
0.208	989.500	12.300	84.0	ABH
0.253	984.200	12.200	84.0	ABH
0.270	982.300	12.900	83.0	ABH
0.365	971.300	16.700	30.0	ABH
0.543	951.400	23.700	6.0	ABH
0.558	949.800	24.300	6.0	ABH
0.771	926.800	25.600	4.0	ABH
1.525	850.000	21.700	7.0	ABH
3.174	700.000	12.400	5.0	ABH
3.182	699.300	12.300	5.0	ABH
4.017	632.100	5.200	14.0	ABH
4.514	594.600	3.900	4.0	ABH
4.974	561.600	0.000	6.0	ABH
4.984	560.900	0.000	5.0	ABH
5.891	500.000	-6.700	7.0	ABH
6.295	474.700	-10.400	11.0	ABH
6.856	441.000	-13.700	6.0	ABH
6.880	439.600	-13.800	25.0	ABH
6.912	437.800	-14.100	8.0	ABH
7.590	400.000	-19.100	4.0	ABH
8.037	376.600	-21.800	5.0	ABH
8.184	369.100	-23.100	10.0	ABH
8.232	366.700	-23.500	36.0	ABH
8.284	364.100	-24.000	14.0	ABH

0.3088 .000 94.842 .000 .000 0.000 1 275.374 T

830 1250 10 10 0

0

Identification Range, RUN 5

F 7 3 1 1 6 6 6 6 6 6 1 1 1 284.70 0.000

3 0 0 16 0 0 27.080 12.04 10.50 .000 .000

29 0 0 Aug. 04 1992, 0441, 0449, STBD

0.007	1013.600	12.200	94.0	ABH
0.025	1011.625	12.280	92.4	ABH
0.050	1008.881	12.390	90.2	ABH
0.075	1005.709	12.499	88.0	ABH
0.120	1000.000	12.700	84.0	ABH
0.208	989.500	12.300	84.0	ABH
0.253	984.200	12.200	84.0	ABH
0.270	982.300	12.900	83.0	ABH
0.365	971.300	16.700	30.0	ABH
0.543	951.400	23.700	6.0	ABH
0.558	949.800	24.300	6.0	ABH
0.771	926.800	25.600	4.0	ABH
1.525	850.000	21.700	7.0	ABH
3.174	700.000	12.400	5.0	ABH
3.182	699.300	12.300	5.0	ABH
4.017	632.100	5.200	14.0	ABH
4.514	594.600	3.900	4.0	ABH
4.974	561.600	0.000	6.0	ABH
4.984	560.900	0.000	5.0	ABH
5.891	500.000	-6.700	7.0	ABH
6.295	474.700	-10.400	11.0	ABH
6.856	441.000	-13.700	6.0	ABH
6.880	439.600	-13.800	25.0	ABH
6.912	437.800	-14.100	8.0	ABH
7.590	400.000	-19.100	4.0	ABH
8.037	376.600	-21.800	5.0	ABH
8.184	369.100	-23.100	10.0	ABH
8.232	366.700	-23.500	36.0	ABH
8.284	364.100	-24.000	14.0	ABH

0.1393 .000 92.182 .000 .000 0.000 1 277.645 T

830 1250 10 10 0

0

Identification Range, RUN 6

F	7	3	1	1	6	6	6	6	6	6	1	1	1	284.70	0.000
	3	0	0	16	0	0	27.080	8.277	10.50	.000	.000				

29   0   0   Aug. 04 1992, 0503, PORT Aspect

0.007	1013.600	12.200	94.0	ABH
0.025	1011.625	12.280	92.4	ABH
0.050	1008.881	12.390	90.2	ABH
0.075	1005.709	12.499	88.0	ABH
0.120	1000.000	12.700	84.0	ABH
0.208	989.500	12.300	84.0	ABH
0.253	984.200	12.200	84.0	ABH
0.270	982.300	12.900	83.0	ABH
0.365	971.300	16.700	30.0	ABH
0.543	951.400	23.700	6.0	ABH
0.558	949.800	24.300	6.0	ABH
0.771	926.800	25.600	4.0	ABH
1.525	850.000	21.700	7.0	ABH
3.174	700.000	12.400	5.0	ABH
3.182	699.300	12.300	5.0	ABH
4.017	632.100	5.200	14.0	ABH
4.514	594.600	3.900	4.0	ABH
4.974	561.600	0.000	6.0	ABH
4.984	560.900	0.000	5.0	ABH
5.891	500.000	-6.700	7.0	ABH
6.295	474.700	-10.400	11.0	ABH
6.856	441.000	-13.700	6.0	ABH
6.880	439.600	-13.800	25.0	ABH
6.912	437.800	-14.100	8.0	ABH
7.590	400.000	-19.100	4.0	ABH
8.037	376.600	-21.800	5.0	ABH
8.184	369.100	-23.100	10.0	ABH
8.232	366.700	-23.500	36.0	ABH
8.284	364.100	-24.000	14.0	ABH

0.1548	.000	93.235	.000	.000	0.000	1	295.427	T
830	1250	10	10	0				
0								

Identification Range, RUN 7

F   7   3   1   1   6   6   6   6   6   6   1   1   1   284.70   0.000

    3   0   0   16   0   0   27.080   8.049   10.50   .000   .000

    29   0   0   Aug. 04 1992,0511, STBD Aspect

0.007	1013.600	12.200	94.0	ABH
0.025	1011.625	12.280	92.4	ABH
0.050	1008.881	12.390	90.2	ABH
0.075	1005.709	12.499	88.0	ABH
0.120	1000.000	12.700	84.0	ABH
0.208	989.500	12.300	84.0	ABH
0.253	984.200	12.200	84.0	ABH
0.270	982.300	12.900	83.0	ABH
0.365	971.300	16.700	30.0	ABH
0.543	951.400	23.700	6.0	ABH
0.558	949.800	24.300	6.0	ABH
0.771	926.800	25.600	4.0	ABH
1.525	850.000	21.700	7.0	ABH
3.174	700.000	12.400	5.0	ABH
3.182	699.300	12.300	5.0	ABH
4.017	632.100	5.200	14.0	ABH
4.514	594.600	3.900	4.0	ABH
4.974	561.600	0.000	6.0	ABH
4.984	560.900	0.000	5.0	ABH
5.891	500.000	-6.700	7.0	ABH
6.295	474.700	-10.400	11.0	ABH
6.856	441.000	-13.700	6.0	ABH
6.880	439.600	-13.800	25.0	ABH
6.912	437.800	-14.100	8.0	ABH
7.590	400.000	-19.100	4.0	ABH
8.037	376.600	-21.800	5.0	ABH
8.184	369.100	-23.100	10.0	ABH
8.232	366.700	-23.500	36.0	ABH
8.284	364.100	-24.000	14.0	ABH

0.1640   .000   92.570   .000   .000   0.000   1   289.911   T

830   1250   10   10   0

0

Identification Range, RUN 8

```
F   7   3   1   1   6   6   6       6       6       6       1       1   1   284.70   0.000
        3   0   0   16  0   0   27.080   7.943   10.50   .000    .000
        29  0   0   Aug. 04 1992, 0522, PORT
```

0.007	1013.600	12.200	94.0	ABH
0.025	1011.625	12.280	92.4	ABH
0.050	1008.881	12.390	90.2	ABH
0.075	1005.709	12.499	88.0	ABH
0.120	1000.000	12.700	84.0	ABH
0.208	989.500	12.300	84.0	ABH
0.253	984.200	12.200	84.0	ABH
0.270	982.300	12.900	83.0	ABH
0.365	971.300	16.700	30.0	ABH
0.543	951.400	23.700	6.0	ABH
0.558	949.800	24.300	6.0	ABH
0.771	926.800	25.600	4.0	ABH
1.525	850.000	21.700	7.0	ABH
3.174	700.000	12.400	5.0	ABH
3.182	699.300	12.300	5.0	ABH
4.017	632.100	5.200	14.0	ABH
4.514	594.600	3.900	4.0	ABH
4.974	561.600	0.000	6.0	ABH
4.984	560.900	0.000	5.0	ABH
5.891	500.000	-6.700	7.0	ABH
6.295	474.700	-10.400	11.0	ABH
6.856	441.000	-13.700	6.0	ABH
6.880	439.600	-13.800	25.0	ABH
6.912	437.800	-14.100	8.0	ABH
7.590	400.000	-19.100	4.0	ABH
8.037	376.600	-21.800	5.0	ABH
8.184	369.100	-23.100	10.0	ABH
8.232	366.700	-23.500	36.0	ABH
8.284	364.100	-24.000	14.0	ABH

```
0.1615   .000   91.687   .000   .000   0.000   1   293.928   T
830           1250    10       10       0
0
```

LIST OF REFERENCES

1. Zeisse C.R., *SeaRad, A Sea Radiance Prediction Code*, Technical Report 1702, Naval Command, Control and Ocean Surveillance Center, RDT and E Division, November 1995.

2. McGrath C.P., *PREOS Program for Determining Detection Range of Airborne FLIR Systems*. Naval Command,Control and Ocean Surveillance Center, RDT&E Division, Technical Report 1448, January 1992. San Diego, CA.

3. Kreitz Jon C., *Preliminary Evaluation of the PREOS Program For Determining Detection Ranges of Airborne FLIR Systems* MS Thesis, Naval Postgraduate School, December, 1992.

4. Hudson, A. D., *Infrared Systems Engineering*, John Wiley and Sons, Inc., NY, 1969.

5. Chappel A., Ed., *Optoelectronics; Theory and Practice*, McGraw-Hill Book Company, 1978.

6. Wood, David S., *Thermistor Validation and Path Radiance Effects in Ship Thermal Image Measurements*, MS Thesis, Naval Postgraduate School, September, 1991.

7. Cooper, A.W., P. L. Walker, and E. A. Milne and B.J. Cook, *Evaluation of Tactical Detection Aid Code Prediction of FLIR Range Performance*, Characterization, propagation and Simulation of Sources and Backgrounds II, Dieter Clement, Wendell Watkins, Editors Proc SPIE 1687,147-156 (1992) .

8. Shumaker, David L., J.T. Wood and C. R. Thacker, *Infrared Imaging Systems Analysis*. The Environmental Research Institute of Michigan, 1993.

9. Hepfer, K. C., *MRT and MDT Function, Navy Surface Warfare Center Program Description*, 1981, Dahlgren, VA.

10. Dodson, Ronald Gene, *A Comparison of FLIR Performance Prediction Models: UFLIR and MKII TDA* MS Thesis, Naval Postgraduate School, September, 1989.

11. Hughes, Herbert G., and Charles P. McGrath, *Surface Ship Infrared Signatures Determined Using an Airborne Imaging System*, San Diego, CA.

12. McGrath, C.P., *A FLIR Case Study Using the EOTDA Mark III*, Naval Command, Control and Ocean Surveillance Center , RDT&E Division, San Diego, CA. 92152.

13. Moser, Paul M., *Mathematical Model of FLIR*, Technical Memorandum NADC-20203:PMM, Aero Electronic Technology Department, Naval Air Development Center, Warminster, Pennsylvania 18974, 19 October 1972.

14. Lloyd, J. M., *Thermal Imaging Systems*, Honeywell Inc. Radiation Center, Lexington, Massachusetts, Plenum Press, New York, 1975.

15. Howe J. D. ,*The Infrared and Electro-Optic System Handbook*, SPIE, Optical Engineering Press, Vol.4, Chapter 2,1993.

INITIAL DISTRIBUTION LIST

No. Copies

1. Defense Technical Information Center   2
8725 John J. Kingman Rd., STE 0944
Ft. Belvoir, VA 22060-6218

2. Dudley Knox Library   2
Naval Postgraduate School
411 Dyer Rd.
Monterey, CA. 93943-5101

3. Professor Alfred W. Cooper   2
Code Ph/Cr
Naval Postgraduate School
Monterey, CA. 93943-5101

4. Prefessor Donald L. Walters   1
Code Ph/We
Naval Postgraduate School
Monterey, CA. 93943-5101

5. Dr. A. Goroch Naval Research Laboratory.   1
Monterey, CA. 93943-5502

6. Naval Command Control and Ocean Surveillance Center   1
RDT&E Division
ATTN : DR. J.H. Richter, Code 54
53570 Silvergate Ave.
San Diego, CA. 92152-5230

7. Naval Command Control and Ocean Surveillance Center   1
RDT&E Division
ATTN : Dr. C. R. Zeisse, Code 543
53570 Slivergate Ave.
San Diego, CA. 92152-5230

8. Liu, Fu-Chau   3
#2, Lane 52, HWA-ER St,
Ping-Tung City, Taiwan, R.O.C.